Analysis of Ice Recrystallization Inhibition Activities among Different Antifreeze Proteins

（異なる不凍タンパク質の間の氷再結晶抑制活性の解析）

By

Anika Tahsin Rahman

(March 2019)

Analysis of Ice Recrystallization Inhibition Activities among Different Antifreeze Proteins

（異なる不凍タンパク質の間の氷再結晶抑制活性の解析）

A dissertation submitted to Division of Life Science, Graduate School of Life Science, Hokkaido University, for the fulfillment of the Degree of Doctor of Philosophy in Life Science

By

Anika Tahsin Rahman

(March 2019)

Transdisciplinary Life Science Course

Division of Life Science

Graduate School of Life Science

Hokkaido University

Sapporo 060-0810, Japan

Contents

Accomplishments

Acknowledgements

List of Figures

List of Tables

List of Abbreviations

ACW	**Anchored clathrate water**
AFGP	**Antifreeze glycoprotein**
AFP	**Antifreeze protein**
bpAFP	**AFP from barfin plaice fish muscle**
CD	**Circular dichroism**
CfAFP	**AFP from *Choristoneura fumiferana***
ColAFP	**Colwellia sp. Strain SLW05 antifreeze protein**
DcAFP	**AFP from *Dendroides Canadensis***
FIPA	**Fluorescence-based ice plane affinity**
FcAFP	**AFP from *Fragilariopsis cylindrus***
FfIBP	***Flavobacterium frigoris* PS1 antifreeze Protein**
IBP	**Ice-binding protein**
IBS	**Ice-binding site**
IR	**Ice recrystallization**
IRI	**Ice recrystallization Inhibition**
iwAFP	**AFP from *Campaea perlata***
LeIBP	**Leucosporidium sp. AY30 antifreeze protein**

LpAFP	**AFP from *Lolium perenne***
lpAFP	**AFP from *Brachyopsis rostratus***
MAXI	**Type Ih AFP from *Pleuronectes americanus***
MD	**Molecular dynamics**
MpAFP	**AFP from *Marinomonas primoryensis***
Mw	**Molecular weight**
NagAFP	**AFP from *Navicula glacei***
nfeAFP	**AFP from notched-fin-eelpout**
nfeAFP6(A20L)	**Mutant version of 6th isoform of AFP from notched-fin-eelpout**
NMR	**Nuclear magnetic resonance**
PDB	**Protein Data Bank**
PVC	**Polyvinyl chloride**
QAE-Sephadex-binding	**Quaternary-amino-ethyl-Sephadex-binding**
RMSD	**Root mean squared deviation**
RTX	**Repeats-In-Toxin**
RiAFP	**AFP from *Rhagium inquisitor***
SDS-PAGE	**Sodium dodecyl sulfate-polyacrylamide gel electrophoresis**

SP-Sephadex-binding	**Sulfopropyl-Sephadex-binding**
TH	**Thermal hysteresis**
Tf	**Freezing Point**
TisAFP8	**8th isoform of AFP from *Typhula ishikariensis***
Tm	**Melting point**
TmAFP	**AFP from *Tenebrio molitor***
UV	**ultraviolet**
sfAFP	**Snow flea antifreeze protein**

Chapter 1

General Introduction

1.1 Proteins:

Proteins are linear polymers of up to 20 different L-α-amino acids. All proteinogenic amino acids have common structural features, including an α-carbon to which an amino group, a carboxyl group, and a variable side chain are bonded. Only proline differs from this basic structure as it contains an unusual ring to the N-end amine group, which forces the CO–NH amide moiety into a fixed conformation.[1] There are 20 different amino acid which can be connected by a peptide bond between the carboxyl group and the amino group in a linear chain called a polypeptide.[2]

1.1.1 Functions of Proteins:

Proteins assist a diverse range of functions within cells. Proteins helps as structural elements, transportation channels, signal receptors, transmitters and enzymes. Different functional groups of proteins are responsible for their definite properties and functions. Each human being has several hundred thousands of different proteins in their body. By folding into secondary, tertiary, and quaternary structures, proteins can obtain on a variety of three-dimensional shapes depending on the amino acid sequence. All proteins possess primary, secondary and tertiary structures but quaternary structures only are formed when a protein is made up of two or more polypeptide chains.[2]

1.2 Life at Extreme Environments:

Organisms inhabiting extreme environments are known as extremophiles. Extremophiles thrive in habitats which for other terrestrial life-forms are hostile or even lethal. They have the ability to thrive in extreme hot niches, ice and salt solutions, as well as acid and alkaline conditions. Extremophiles are survived according to the conditions in which they grow: as thermophiles and hyperthermophiles can grow at high or very high temperatures respectively. In contrast psychrophiles are organisms that grow best at low temperatures. Acidophiles and alkaliphiles are optimally adapted to acidic or basic pH values respectively[3].

1.2.1 Strategies to Survive in Cold Environment:

Above three-quarters of the Earth's surface is cold. About 70% of the Earth`s surface is covered with oceans that have a constant temperature of 4-5 °C below a depth of 1,000m. Psychrophiles living in such extremely cold environments have developed a set of behavioral, physiological and molecular level adaptations to help them overcome extremely cold temperatures. The behavioral level adaptations play a key role which encompasses long distance migration or escaping of organisms in local shelters, for instance within tree bark crevices or under snow cover. Molecular level adaptations include productions and using of poyols, ice nucleatores or antifreeze are considered as molecular level adaptations [4,5,6]. These molecules act colligatively or non-colligatively to depress the freezing temperature of body fluids. Antifreeze proteins is a member of a group named ice binding protein involved in depressing the freezing temperature of the body fluid in a non-colligative manner[7].

1.3 Ice binding Proteins (IBPs):

Ice binding proteins (IBPs) are able to specifically interact with ice crystal to modulate their growth below melting point of the solution[8]. The first IBP was identified in 1969 from Antarctic Notothenioid fish[9]. Later it was found to be produced by insects, microorganisms and plants[8]. The sole ability of IBPs to modify ice crystal growth also holds great promise for a range of application areas including food technology, materials science, and biomedicine. So far four different types of roles of IBPs have been identified; antifreeze, ice recrystallization inhibition, ice structuring and ice adhesion[8].

1.4 Functional Diversities of Ice binding Proteins (IBPs):

1.4.1 Antifreeze:

Antifreeze activity is the most important role of IBPs found in freeze-avoiding species like fish as it allows to prevent further growth of endogenous ice crystals circulating in their blood stream or hemolymph. The activity is quantified by the temperature range in which ice crystal growth is effectively blocked[8]. AFP adsorption increases local curvatures in the ice front, which is energetically less favorable for water molecules to add to the ice lattice. It ultimately

results in a non-colligative depression of the freezing point and a slight elevation of the melting point due to the Gibbs-Thompson effect[10].

The antifreeze activity of IBPs also allows to modify ice crystal morphology which remains unchanged within the TH gap. Elongated hexagonal bipyramid shaped ice crystal are usually formed with moderate activity of IBPs whereas hyperactivity induces varied ice crystal shapes. For example, TmAFP from *Tenebrio moilitor* induces lemon shaped ice crystal and CfAFP from *Choristoneura fumiferana* produces hexagonal disc shapes[11].

1.4.2 Ice Recrystallization:

Ice recrystallization is a thermodynamically driven, spontaneous process in which ice crystals in a solution tend to become large at the expense of smaller ones. This causes in a decrease in the grain boundary area per unit volume of ice, thereby lowering the free energy of the system[8]. IBPs can inhibit recrystallization at very low, micromolar concentrations[12]. This inspired the design of biomimetic antifreezes for use in biomedical applications such as red blood cell preservation[13,14].

1.4.3 Ice Nucleation:

When a solution is super-cooled below the melting point or (equilibrium) freezing point, it remains in the liquid state until the "supercooling point" or "nucleation temperature" is reached. At this temperature, ice-like aggregates of large size form nuclei and result in freezing[15]. In the presence of ice nucleating proteins (INPs), ice nucleation temperature is elevated. The ice binding site of INPs provides a platform for the organization of water molecules in an ice like lattice which favors nucleation[8].

1.4.4 Ice Adhesion:

Recently one IBP, named MpAFP is identified as an ice adhesion. The AFP isolated from Antarctic Gram negative bacteria, *Marinomonas primoryensis* is a large protein and shows Ca^{2+} dependent antifreeze activity[16,17]. The protein is divided into five distinct regions. The N-terminal region I (RI) is responsible for binding the protein to the outer membrane of

bacterium[18]. Region II (RII) project the ice binding domain (RIV) away from the bacterial cell surface in order to bind *M. primoryensis* to the ice abundant[19]. Region IV (RIV) serve to adhere to the underside of ice. Region V (RV) contains RTX-like repeats and may be responsible for directing the protein out of the bacterial cell[18].

1.5 Diversities of AFPs:

AFPs represent different types of diversities structurally and functionally which are describes shortly below.

1.5.1 Structural Diversities of AFPs:

Dozens of 3D structures of AFPs from polar fish, insects, plants, algae, fungi and bacteria have been reported through nuclear magnetic resonance (NMR) and X-ray crystallography experiments. AFPs are found to have a remarkable divergence in their amino acid sequence and tertiary structure despite they share a common function of ice binding. The extraordinary structural diversity might have resulted from convergent evolution in which AFPs arose independently from diverse progenitors in different organisms to protect themselves under strong selective pressure[20, 21]. Different features of their 3D structures have allowed to classify AFPs into several types which are described below

1.5.1.1 Fish AFPs:

About five decades ago, the first fish AFP termed antifreeze glycoproteins (AFGPs) was discovered from Nototheoid fishes. AFGPs are composed of repeats of a simple glycotripeptide monomer (Thr-Ala/Pro-Ala-) with a disaccharide attached to each threonine residue[22]. The presence of this protein at millimolar concentration has allowed the Nototheoid fishes to stop ice growth efficiently[23].

Most of the fish AFP represent TH activities of 0.5-1.5°C at millimolar concentration. Currently, fish AFPs have been classified into five types [AFP type I-IV and AFGP]. Among these AFPs, the NMR and/or X-ray derived structures of type IV AFP and AFGP are yet to be discovered.

The very first Type I AFP identified from winter flounder (*Pseudopleuronectes americanus*). The type I AFPs are usually long, simple alanine-rich amphipathic α-helices with the molecular weight of ca. 3.3kDa[24,25]. The plasma of winter flounder pseudomonas expresses another type I AFP homologue[26]. The X-ray crystallography experiment of this protein showed a homodimeric, four helix-bundled structure. The four monomer units of the bundle is stabilized by numerous hydration water molecules[27].

Type II AFPs are cysteine-rich disulfide-stabilized globular proteins[22]. It shows a high similarity to the carbohydrate-recognition domain of C-type lectins (Mw ~14 kDa). The protein is classified into two types by having dependency on Ca^{2+} ion on its activity. The type II AFP isolated from sea raven (*Hemitripterus americanus*) shows Ca^{2+} independency whereas the AFPs from smelt (*Osmerus mordax*) and Atlantic herring (*Clupea harengus*) represent ca dependency in exhibiting the activity[22].

The type III AFPs are composed of several short ß-strands connected by large loops. It was firstly discovered in ocean pout (*Macrozoarces americanus*)[28,29].

Type IV AFP are Gln-rich, highly helical and have a four-helic bundle structure[30]. The blood plasma of longhorn sculpin (*Myoxocephalus octodecimspinosis*) expresses type IV AFP[8]. The protein is composed of 108 amino acid residues with a molecular weight of 12.3 kDa[31].

1.5.1.2 Arthropod AFPs:

The first AFP from arthropod was reported in yellow mealworm *Tenebrio molitor*. With a molecular weight of 8.4 kDa, the AFP is characterized by its rich content of Thr- and Cys residues. The AFP folds into a right handed ß-helix and consist of seven tandem 12-residue repeats. The Thr-X-Thr (T-X-T) pattern on each ß-strand of one side of helix represents the ice-binding site (IBS) of the AFP[32].

The moth, spruce budworm (*Choristoneura fumiferana*) produces a 9 kDa AFP which is also rich in Thr- and Cys- residues like TmAFP. The AFP folds into a left-handed ß-helical structure. The IBS of the AFP also contains T-X-T motif like TmAFP[33,34,35].

The larvae of the pale beauty moth *Campaea perlata* shows a TH activity of 6.4 °C due to expression of two AFP isoforms with a molecular weight of 3.5 and 8.3 kDa. The 8.3 kDa AFP isoform has flat silk-like ß-helix in its model structure[36].

One member of snow flea arthropod group, named *Hypogastrura harveyi* displays a TH activity of 5.8 °C in its body extract. The hyperactivity of the extract is due the presence of two types of AFP (sfAFP) isoforms with a molecular weight of 6.5 and 15.7 kDa[37]. The X-ray structure of the small isoform showed that it is composed of six antiparallel left-handed polyproline II-like helices. The helices are stacked in two sets of three to form a compact brick like structure with one hydrophilic face and one hydrophobic face[38]. The structure of larger isoform is amphipathic in nature with a hydrophilic surface on one side and hydrophobic, putative ice-binding surface on the other. It has 13 polyproline II-like helices connected by proline-containing loops stacked into two flat sheets oriented antiparallel to one another[39].

The RiAFP, produced by the longhorn beetle, *Rhagium inquisitor* is a 13 kDa molecule, shows TH of around 6.5 °C. The x-ray crystal structure of the AFP shows its flat, silk-like ß-helical (solenoid) structure like the model structure of wiAFP[40,41].

Recently, an AFP was discovered from Lake Ontario midge (*Chironomidae*). The major isoform of this midge AFP has a 10 residue tandem repeating sequence xxCxGxYCxG with regularly spaced cysteines, glycines and tyrosine residues. Its structure is modeled as a tightly wound left-handed solenoid fold, in which 16 cysteine residues are disulfide bonded to brace the solenoid coil[42].

1.5.1.3 Bacterial AFPs:

The bacterial IBP gene was firstly identified in sea ice gram-negative bacterium *Colwellia* strain SLW05[43]. Further study revealed the existence of proteins which are similar to IBPs in many sea ice bacteria *Polribacter irgensii* (ZP 0118128; sequence identity: 61%, sequence similarity: 75%), *Psychromonas ingrahamii* (ZP 01349469; sequence identity: 59%,

sequence similarity: 71%), and marine bacterium *Shewanella frididimarina* (YP 749708; sequence identity: 52%, sequence similarity: 69%)[22].

The plant growth promoting rhizobacterium, *Pseudomonas putida* was reported to be capable of producing an AFP with a Mw of ca. 164 kDa having low TH activity (0.1 °C)[44,45]. Moraxella sp was found to produce a 52 kDa protein possessing low TH activity[46]. Additionally, *Pseudomonas fluorescens* was identified for expressing an 80-kDa AFP with very low TH activity[47].

MpAFP (34 kDa by itself) isolated from an Antarctic lake bacterium, *Marinomonas primoryensis* is the first bacteria whose structural characteristics was analyzed. It is found to be a part of large (1.5 MDa) protein found in the cell surface of the bacterium[22]. The X-ray crystal structure of the 34 kDa part of MpAFP showed that the protein has ß-helical fold containing xGTGND repeat motif in every turn as IBS. The IBS of the protein contains an array of ice like surface waters that are anchored by hydrogen bonds directly to the polypeptide backbone and adjacent side chains[48,18].

A moment ago, the Antarctic bacterium *F. frigoris* PS2 on the shore of McMurdo Sound (GenBank accession no. AHK00000000.1) was identified and characterized for expressing an IBP named FfIBP[49,50]. The IBP has an 56% sequence similarity with LeIBP and 10-fold higher antifreeze activity than it. The FfIBP has a regular motif (T-A/G-X-T/N motif) and more regularly aligned ice-binding residues on its IBS than LeIBP[51].

In 2014, the structural data of *Colwellia* sp. Strain SLW05 (ColAFP) revealed its -helical structure like LeIBP, TisAFP and FfIBP[52,53].

Additionally, Antarctic psychrophilic marine ciliate *Euplotes focardii* was identified for possessing two sequences encoding IBPs designated as EFsymbAFP and EfsymbIBP . The N-terminal 23 residue deleted EFsymbAFP has TH activity of 0.53 °C at 50 μM and IRI activity at nanomolar range[54,55].

1.5.1.4 Fungal AFP:

To date, the detailed analysis of genomic and antifreeze properties are done for two mishrooms (enoki and shiitake), one snow mold fungus (*Typhula ishikariensis*) and two yeast organisms (*Glaciozyma Antarctica* and *Glaciozyma* sp. AY30)[56–59]. LeIBP expressed in *Glaciozyma* sp. AY30 has a right handed β-helical structure and a TH activity of 0.42 °C[22]. The snow mold fungus (*Typhula ishikariensis*) was identified for expressing seven antifreeze protein isoforms. Of the seven isoforms, TisAFP6 displayed moderate activity and TisAFP8 showed hyperactivity[22].

Four α-helices was identified in *Glaciozyma Antarctica* AFP (Afp1) where each of helical peptide has antifreeze activity[60]. In 2014, another *Glaciozyma Antarctica* AFP (Afp4) was identified which has 93 % amino acid similarity with LeIBP and has a TH activity of 0.8 C at 5 mg/ml concentration[22].

1.5.1.5 Diatom AFP:

AFP genes were also discovered from many polar sea diatoms (Chaetoceros neogracile, Berkeleya sp., Navicula sp., Fragilariopsis sp., and Nitzchia frustulum). Thus AFP genes are playing important role in environmental adaptations of diatoms[22].

1.5.1.6 Plant AFPs:

Freeze tolerant organisms produce AFPs with low TH activity and high IRI activity[61]. These characteristics help to minimize the damages occur due to ice recrystallization. A DcAFP isolated from a common vegetable carrot (*Daucus carota*) is consist of 24-amino acid tandem repeats. The AFP is able to inhibit ice recrystallization even at 1 μg/ml concentration[62,63]. The lpAFP from perennial ryegrass (*Lolium perenne*) is extremely a heat-stable protein with 118 amino acid residues which folds into a left ß-roll structure with eight 14- and 15- residue coils. The AFP shows high IRI activity along with low TH activity[61,64].

1.5.2 Functional Diversities of AFPs:

AFPs` two properties: ability of depressing equivalent freezing temperature below melting point of solution (thermal hysteresis; TH) and ability of inhibiting formation of large ice

crystals at expense of small ice crystals (ice recrystallization inhibition activity; IRI). TH allows to protect polar fish or insects from inoculative freezing of their blood plasma or hemolymph whereas IRI in plant and bacteria prohibits larger ice crystal formation which eventually provide tolerance against freezing[65].

AFPs are classified into two categories: moderately active and hyperactive based on TH activity. The moderately active AFPs exhibit TH values around 0.5 °C to 1.0 °C at millimolar concentrations. AFPs of fish usually exhibit maximal TH of ~2 °C and are considered as moderately active. Usually, all fish, plant AFPs, antifreeze glycoproteins and midge AFP are classified as moderately active AFP. AFPs, able to exhibiting TH ~6 °C at maximum are termed as hyperactive AFPs. The TmAFP isolated from meal-worm beetle is considered as the first reported hyperactive AFP[66,67]. Moreover, arthropod AFPs (CfAFP, iWAFP, sfAFP and RiAFP), a fish AFP (type Ih), bacterial AFP (MpAFP, FfIBP and ColAFP), a fungal AFP (TisAFP8) and a diatom AFP (NagAFP) are reported as hyperactive AFPs[26,43,49,52].

The moderately active AFPs direct ice crystal growth along the c-axis when TH is exceeded whereas hyperactive AFPs allows growth along a-axes[68,34]. Both types of AFPs show concentration dependency in exhibiting TH activity[65]. The affinity towards specific ice planes played an important role in earlier work in exhibiting specific type of TH values in each category of AFP[69].

1.6 Ice Binding Mechanism of AFPs:

AFPs can recognize embryonic ice crystals in excess (55M) of liquid water for adsorbing to ice crystal and arresting their growth[67]. Many mechanisms demonstrating AFP binding to ice have been proposed using experimental and computational data which are described below:

1.6.1 Hydrogen Bonding:

After analyzing X-ray crystal structure of wfAFP, authors proposed a mechanism of antifreeze protein binding to ice surfaces which demonstrated the importance of hydrogen bond formation involving regularly spaced polar side chains (mainly Thr) of the helix.[24]

1.6.2 Hydrophobic Interaction:

Mutagenesis study of AFPI involving mutation of central two Thr residues with Val or Ser provided the existence of hydrophobic interaction. Although the Val mutant had comparable activity like the wild type, the Ser mutant was unable to exert any activity[28,70–72]. So these data recommend that hydrophobic interaction is also significantly important in contribution of adsorption of AFP to ice surface. The release of constrained water on IBS into the bulk solvent results in a gain of large entropy which ultimately drives the binding of AFPs to ice.

1.6.3 Anchored Clathrate Water:

The hypothesis of anchored clathrate water was proposed by Nutt and Smith which was later established by Garnham et al. According to the hypothesis, water molecules of aqueous solution around each AFP IBS are more ordered and experiences slowed dynamics at low temperature. The ordered water molecules are in ice like arrangement which merge with quasi liquid layer waters and convert to ice. It eventually facilitates the binding of AFPs[73,48]. The hypothesis was found to be supportive for explaining X-ray structures of MpAFP and ColAFP. In MpAFP, four MpAFP molecules were packed within the unit cell of crystal structure. Aligned ice like water molecule structures were formed due to hydrophobic effect by the relative hydrophobicity of the IBS which were then anchored to AFP via hydrogen bonds. The anchored waters match well with the basal and primary prism plane of ice. The mechanism was termed as anchored clathrate water mechanism[48]. Recently, ordered water molecules were discovered in the interior structure of MAXI which are hypothesized to be helpful in stabilizing four helix bundle. The water molecules are thought to extend towards protein surface to be involved in ice binding through ACW mechanism[27].

In the crystal structure of QAEI isoform of type III AFP, the primary prism plane IBS was partially exposed to solvent, of which five water molecules were ice like[74]. The pyramidal plane IBS was involved in crystal packing. Sun et al. exposed the pyramidal plane IBS by fusing type III AFP from *Macrozoarces americanus* with maltose binding protein[75]. By combining with molecular dynamics simulations, waters on IBS were exposed which matched well with their target planes.

1.7 Ice Plane Binding Ability of AFPs:

The ice-etching technique established by Knight et al. allowed the identification of ice planes to which AFPs bind. The technique involves attaching a single ice crystal of known orientation to a temperature-controlled brass cold finger which is followed by immersing the ice crystal into an insulated container of dilute AFP solution. After allowing growth to a certain size of hemisphere (ca 6 cm in diameter), the ice crystal is removed and taken to a cold room. The surface of ice crystal is scrapped to remove residual AFP and kept there for several hours for evaporation. After completion of all the steps, AFP bound areas appear as white etched patches whereas AFP-non-bound areas show mirror smooth appearance[10].

The above described method has been further modified by Garnham et al. involving using of AFPs fluorescently labeled with a chimeric tag or a covalent dye. The authors termed the method as Fluorescent based ice plane affinity[76].

The ice-plane specificity of different AFPs has been examined using the mentioned techniques. The type I, winter flounder HPLC6, wfAFP and Alaskan plaice AFP have shown affinity towards pyramidal planes whereas another type I AFP from sculpin binds towards secondary prism planes[10,77]. The type Ih AFP from winter flounder, Maxi has shown multiple ice plane specificity including the basal planes[27]. The type II lpAFP from Long-snout poacher binds towards prism and pyramidal planes[78,77]. The type III AFP from Notched-fin eelpout gets adsorbed onto primary prism plane and pyramidal plane[76,77].

1.8 Ice Shaping Ability of AFPs:

Normally, ice crystals experience a uniform growth pattern in its all planes except the basal plane leading to formation of a disc like structure. But AFPs have the ability to get adsorbed onto specific ice planes. The AFP bound planes have micro curvatures between ice bound-AFP molecules which provide thermodynamically less favorable conditions for further ice crystal growth[79,80]. Such terminated growths towards specific ice planes give arise of a particular ice crystal morphology. The type I and type II AFPs cause the formation of hexagonal bipyramid shaped ice crystal[81,82]. On contrary, Maxi causes the formation of lemon shaped ice crystal[37].

1.9 Ice as a Heterogeneous Ligand:

Ice can form numerous crystalline forms. But at normal atmospheric pressure and 0 °C temperature, ice can form hexagonal ice with six fold symmetry. The structure has been confirmed using X-ray diffraction study. It showed different patterns of oxygen atoms on the surface of distinct ice planes which are defined by Miller-Bravais indices. The reciprocal of the distances from the center of the unit cell to where they intersect each axes is considered as each planes (a_1, a_2, a_3 and c). In a hexagonal ice, the basal planes intersect the a-axes at infinite distances and the c-axis at 1. The reciprocals of infinite and 1 are 0 and 1 respectively. By considering the Miller-Bravais index, the basal plane is designated as (0001). The primary and secondary prism planes cut the c-axis at infinity. The primary prism plane, parallel to the sides of hexagonal unit cell is designated as (01-10). The secondary prism plane is perpendicular to a-axes and is considered to have indexes, such as (2-1-10). The unit cell is interested at different angles by pyramidal planes. The planes have indexes such as, (1-101) or (1-102)[80].

1.10 Purpose and Scopes:

Recrystallization refers to the growth of the larger crystals at the expense of the smaller ones[8]. Here, the interfacial energy is the driving force of the phenomenon[83]. The process of recrystallization has great importance in fundamental research and practical applications[84]. The modification of ice crystal sizes through recrystallization occurs during storage and

transport of frozen foods. It ultimately reduces the advantages obtained by quick freezing and inducing physicochemical changes which changes their quality and shorten their shelf life[83].

The mechanism of inhibition and factors determining the strong IRI efficiencies remains still challenging, instead of development of many tools and software to appreciate thousands of ice grains in photomicroscope snapshots[85–90]. The present work recrystallization is based on analyzing direct microscopic observation of ice crystals in 40% sucrose where 13-15 ice crystals exhibiting only uniform growth were examined from a video file. The IRI efficiency parameters obtained from the method for different AFP species were ultimately compared with the previous knowledge of their ice-binding properties. Type I-III AFP, a defective isoform of Type III AFP and a fungal AFP named Tis8 were selected for the analysis due their ability of covering ice surface in different amount. The specific objectives in each following chapter are as follows:

Chapter 2. The brief discussion regarding the purifying analyzed proteins were done here. The chapter mainly focused on examining the IRI efficiency of type I-III AFPs, a defective isoform of type III AFP and a fungal AFP isoform from *Typhula ishikariensis* (Tis8) with our modified "sucrose-sandwich splat assay" where uniform growth of 13-15 ice grains were only analyzed to evaluate IRI rate. The validity of modified method was also shown through measuring the "ice volume fraction". The IRI rate of each AFP at different concentrations were measured. The IRI activity of native AFGP sample was also analyzed.

Chapter 3: The ice-binding properties of each AFPs were examined through analyzing TH activity and fluorescence based ice plane affinity (FIPA) experiments which were later compared with their respective IRI efficiency. At last, sizes of ice-binding site of each type of analyzed AFPs as well as their ice shaping activities were also discussed.

Chapter 4. The chapter focused on compiling all IRI data obtained through our analysis or previous work. The data were compared with each other to understand the "ice

recrystallization process" more clearly. Here, the effects of using different solutes on ice recrystallization kinetics was also discussed.

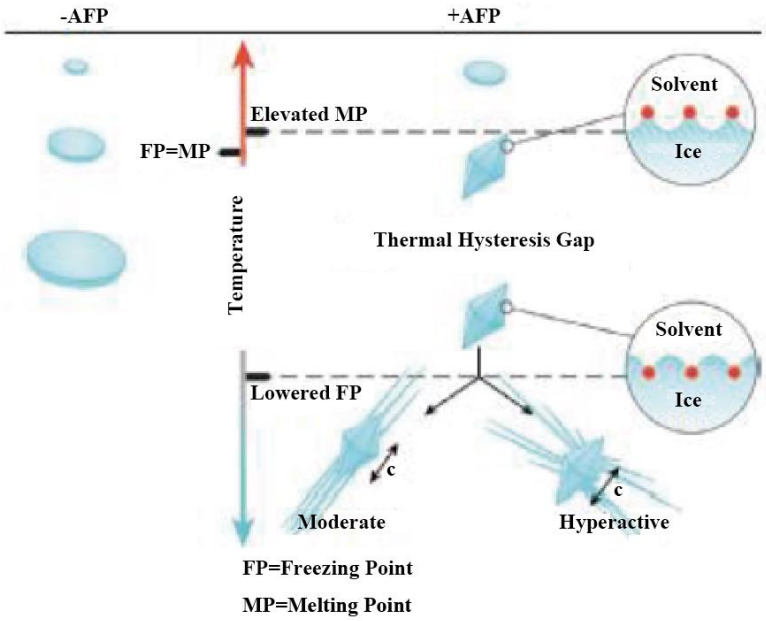

Figure 1.1: Thermal hysteresis. Left of the vertical temperature scale shows the situation where antifreeze proteins (AFP) are absent and the freezing point (FP) is the same as the melting point (MP). Ice crystals (light blue disks) shrink or grow beyond this equilibrium temperature. The right-hand side illustrates the ability of AFPs (red dots) to shape ice into a faceted crystal, lower the FP and raise the MP by surface adsorption to ice. The direction of ice growth below the FP is shown in the presence of moderate and hyperactive AFPs in relation to the c-axis of their crystals.

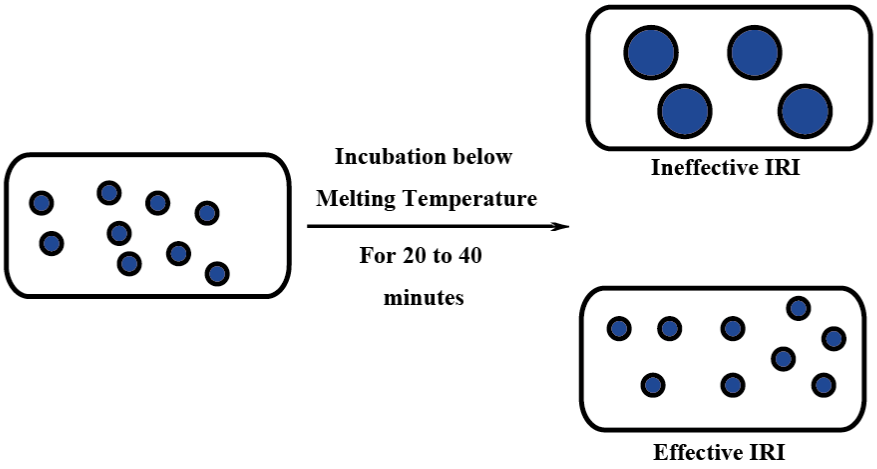

Figure 1.2: Schematic representation of effective and ineffective ice recrystallization inhibition. Ice crystals are represented by the blue spots.

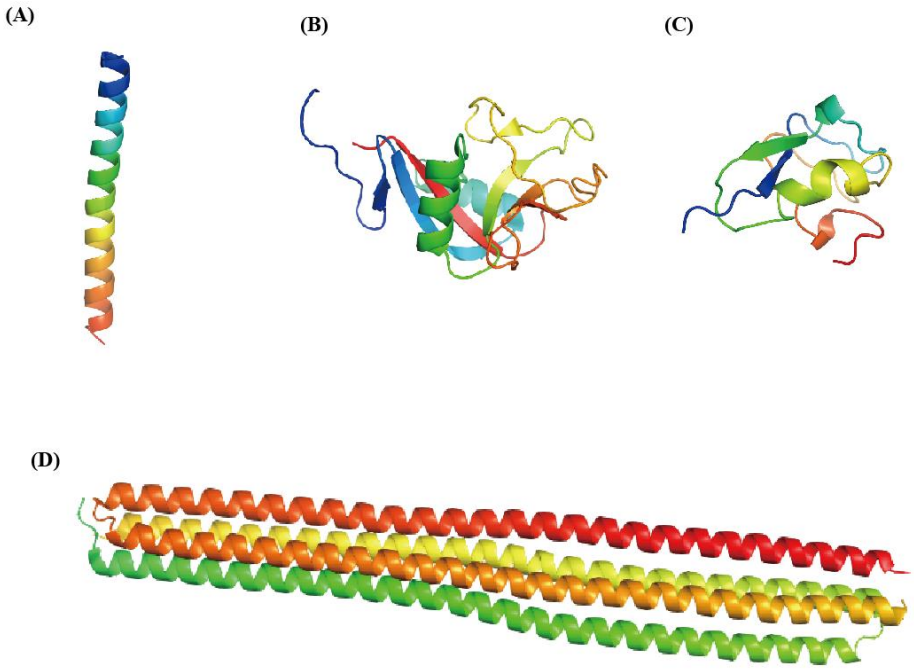

Figure 1.3: X-ray crystal structure of type I, II, III and Ih fish AFPs. X-ray crystal structure of (A) type I AFP (wfAFP) from *Pseudopleuronectes americanus* (regenerated from PDB ID: 1WFB), (B) calcium independent type II AFP (lpAFP) from *Brachyopsis rostratus* (regenerated from PDB ID: 2ZIB), (C) type III AFP from *Zoarces americanus* (regenerated from PDB ID: 1AME) and (D) type Ih AFP from *Pseudopleuronectes americanus* (regenerated from PDB ID: 4KE2). These structures were regenerated using PyMOL[1,91,78,22].

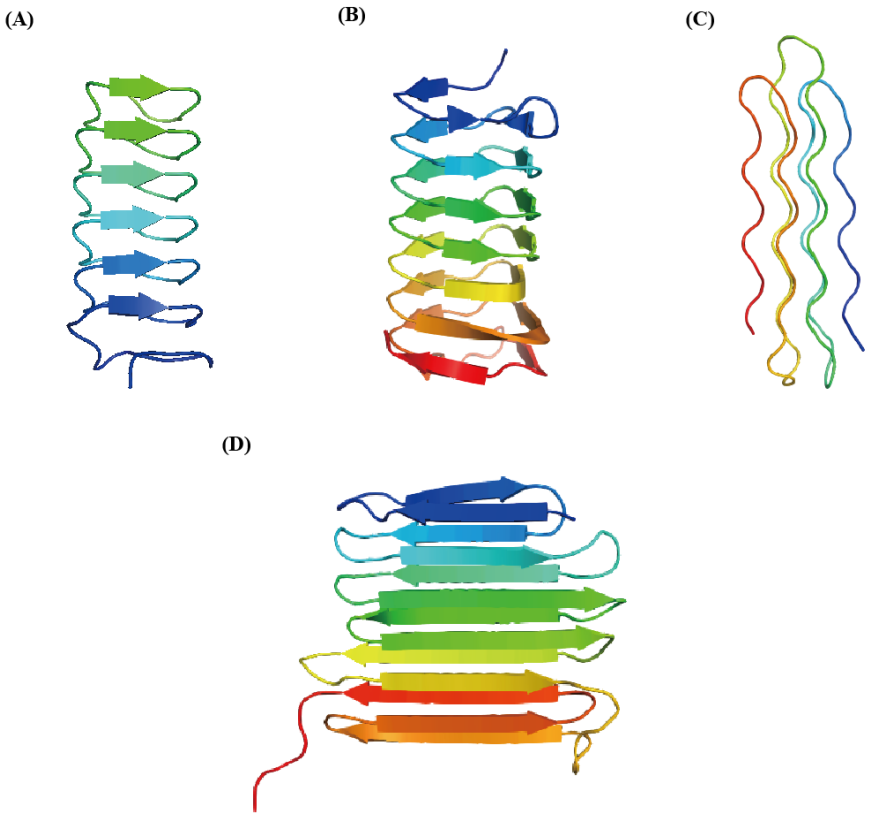

Figure 1.4: X-ray crystal structure of arthropod AFPs. X-ray crystal structure of (A) TmAFP from yellow mealworm (*Tenebrio moliter)* (regenerated from PDB ID: 1E2Z), (B) cfAFP from spruce budworm (*Choristoneura fumiferana*) (regenerated from PDB ID: 1M8N), (C) sfAFP from snow flea arthropod (*Hypogastrura harveyi)* (regenerated from PDB ID: 2PNE), (D) RiAFP from longhorn beetle, (*Rhagium inquisitor)* (regenerated from PDB ID: 4DT5). These structures were regenerated using PyMOL[22].

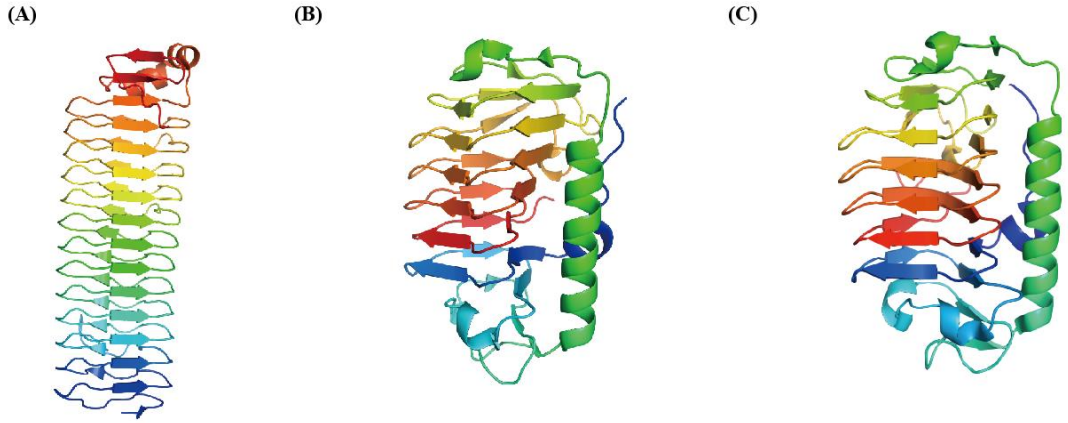

Figure 1.5: X-ray crystal structure of bacterial AFPs. X-ray crystal structure of (A) MpAFP from *Marinomonas primoryensis* (regenerated from PDB ID: 3P4G), (B) FfIBP from *Flavobacterium frigoris* PS I (regenerated from PDB ID: 4NU2), (C) ColAFP from *Colwellia* sp. strain SLW05 (regenerated from PDB ID: 3WP9). These structures were regenerated using PyMOL[22].

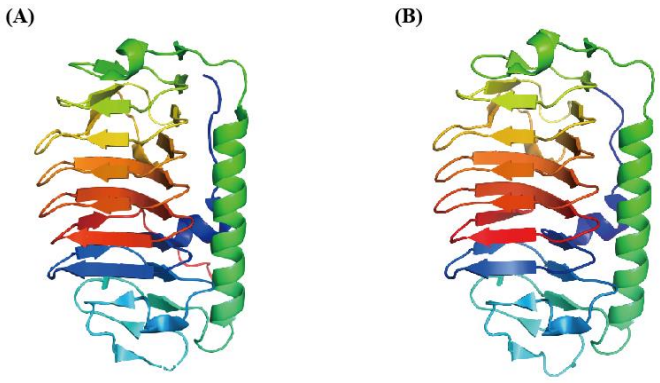

Figure 1.6: X-ray crystal structure of fungal AFPs. X-ray crystal structure of (A) LeIBP from *Glaciozyma* sp. AY30 (regenerated from PDB ID: 3UYU), (B) TisAFP8 from *Typhula ishikariensis* (regenerated from PDB ID: 5B5H). These structures were regenerated using PyMOL[22].

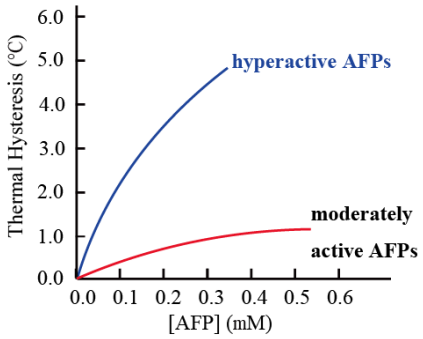

Figure 1.7: Schematic representation of a TH graph showing the difference in TH between two classes of AFPs. The blue line shows TH of hyperactive AFPs, and the red line for moderately active AFPs.

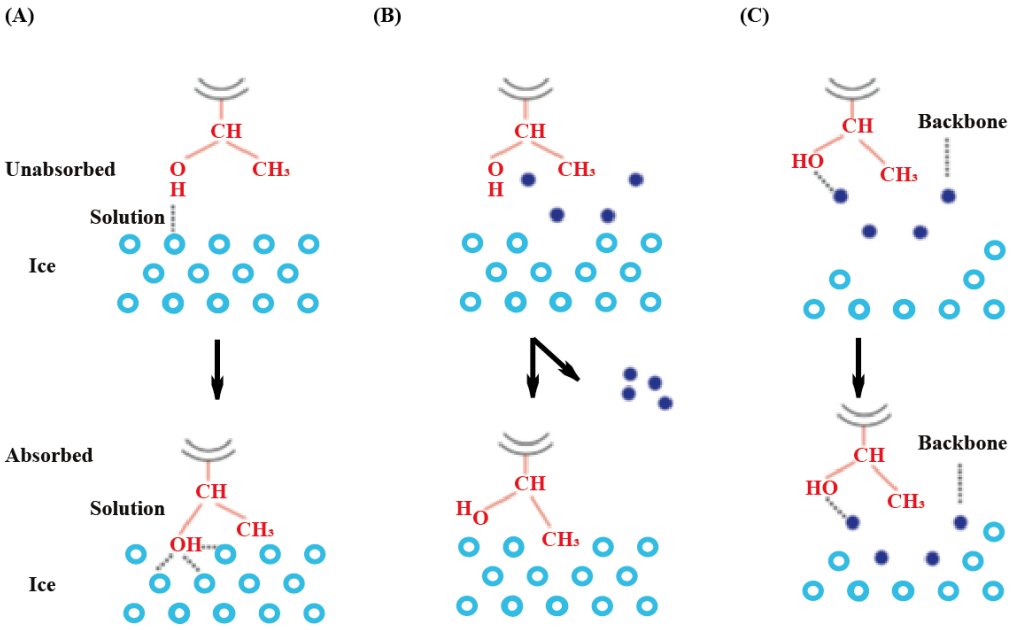

Figure 1.8: Proposed mechanisms for ice-binding proteins (IBP) binding to ice. Three proposed mechanisms for ice binding (panels A, B, and C) are illustrated in the preadsorbed (top) and adsorbed (bottom) states. The ice-binding site (IBS) of an IBP is represented by the single threonine residue in red. Water molecules in the ice lattice or quasi-liquid layer above ice are shown as blue circles. Clathrate waters around the IBS are dark blue dots. (A) Hydrogen bonding hypothesis. Threonine representing the IBS initially hydrogen bonds (broken line) to ice (top), and progresses to have the threonine hydroxyl occupy an ice lattice O atom site to make additional hydrogen bonds. (B) Hydrophobic effect. Constrained waters around hydrophobic groups on the IBS (top) are released into the solvent on IBP binding to ice with an intimate fit (bottom). (C) Anchored clathrate hypothesis. Ice-like clathrate waters around hydrophobic groups on the IBS hydrogen bond to the protein backbone and side chain groups (top). These clathrate waters merge with the quasi-liquid layer waters and become ice (bottom). The structural and mechanistic relationship between ice-binding proteins and ice nucleation proteins.[92]

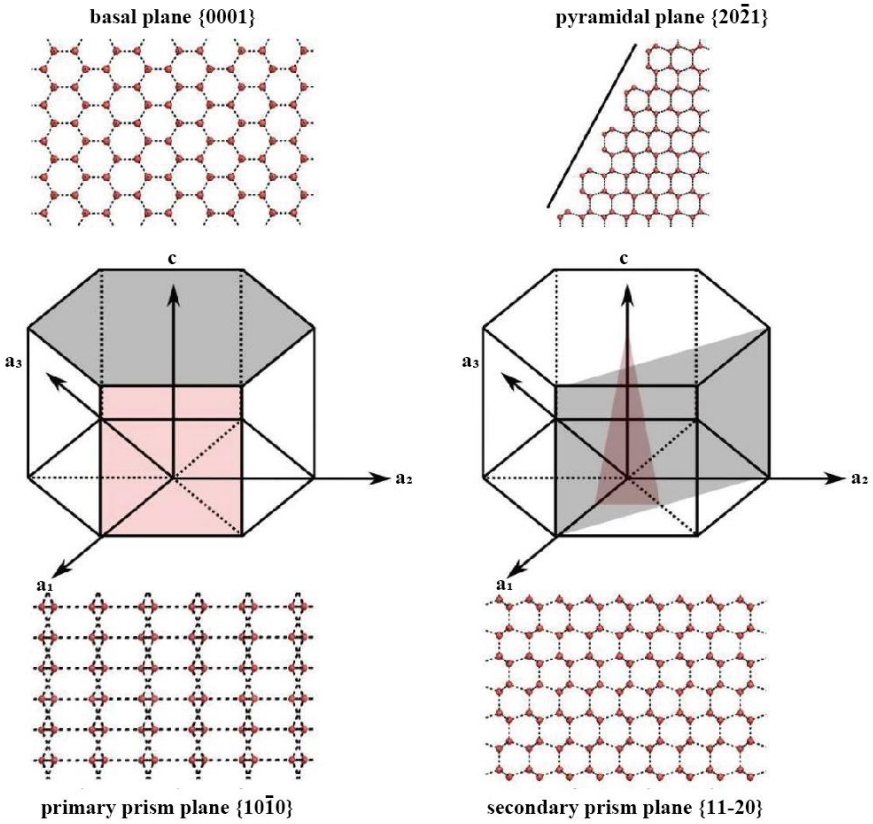

Figure 1.9: Hexagonal unit cell of ice and corresponding ice surfaces. The c and a axes of the unit cells are labelled. The one on the left shows the basal plane (shaded grey) and the primary prism plane (shaded red). The unit cell on the right shows a pyramidal plane (shaded red) and the secondary prism plane (shaded grey). The Miller indices of each plane are indicated, as are the oxygen atoms (red spheres) that constitute each plane. Hydrogen bonds are shown as black hatched lines.[93]

Table 1.1: Ice planes preferentially bound by individual AFPs. AFP-binding planes of ice determined are indicated by the symbol of (+). All planes are marked from TmAFP to ColAFP, which shows the uniform binding of those AFPs to ice hemispheres observed in FIPA analyses.

AFP type	1st Prism	2nd Prism	Pyramidal	Other	Basal
Fish type I (wf)			+		
Fish type I (ss)		+			
Fish type I (bp)		+	+		
Fish type II	+				
(Ca^{2+}-in)					
Fish type II		+			
(Ca^{2+}-de)					
Fish type III	+		+		
Fish type IV				+	
Fish AFGP	+				
LPIBP	+				+
LeIBP	+				+
TisAFP6				+	+
TisAFP8	+	+	+	+	+
TmAFP	+	+	+	+	+
CfAFP	+	+	+	+	+
sfAFP	+	+	+	+	+
RiAFP	+	+	+	+	+
MpAFP	+	+	+	+	+
ColAFP	+	+	+	+	+

Abbreviations used in this table: wf, winter flounder; ss, shorthorn sculpin; Ca^{2+} -in, Ca^{2+} -independent; Ca^{2+} -de, Ca^{2+} -dependent.[69,10,94,78,76,95,96,64,97,98,39,99,48,52,100]

Table 1.2: The basic properties of different AFPs.

Specific name	Organism	TH (°C) [AFP conc]	Mw (Da)	Locality
Fish type I (wf1)	*Pseudopleuronectes americanus*	0.6 [1.4 mM]	3 kDa	Recombinant
Fish type I (ss3)	*Mysocephalus Scorpius*	2.3 [0.03 mM]	3.2 kDa	Recombinant
Fish type I (bp)	*Liposetta pinnifasciata*	1.0 [6.25 mM]	3.2 kDa	Okhotsk coastal area of Japan
Fish type II				
(Ca^{2+}-in)	*Brachyopsis rostratus*	0.5 [0.25 mM]	14 kDa	Northeast coast of Japan
Fish type II				
(Ca^{2+}-de)	*Clupea harengus*	0.4 [0.55 mM]	14 kDa	Recombinant
Fish type III	*Macrozoarces americanus*	0.5 [0.25 mM]	7 kDa	Recombinant
Fish type IV	*Myxocephalus octodecimspinosis*	0.5 [2 mM]	12.3 kDa	Northern coastal waters
Fish $AFGP_{1-5}$	*Fish antifreeze glycoproteins$_{1-5}$*	0.2 [0.04 mM]	15 kDa	Sea ice in Antarctica
LPIBP	*Lolium perenne*	0.5 [0.3mM]	13.8 kDa	Recombinant
LeIBP	*Leucosporidium sp. AY30*	0.4 [370 µM]	25 kDa	Pond in Arctic
TisAFP6	*Typhula ishikariensis*	0.5 [0.3 mM]	23 kDa	Recombinant
TisAFP8	*T. ishikariensis*	2 [180 µM]	23 kDa	Recombinant
TmAFP	*Tenebrio molitor*	3.2 [0.2 mM]	8.5 kDa	Recombinant
CfAFP-501	*Choristoneura fumiferana*	5.5 [0.1 mM]	9 kDa	Recombinant
sfAFP	*Hypegastrura harvveyi*	4.5 [0.03 mM]	15.7 kDa	Recombinant
RiAFP	*Rhagium inquisitor*	6.2 [0.8 mM]	12.8 kDa	Longhorn beetles
MpAFP	*Marinomonas primoryensis*	2 [0.01 mM]	1.5 MDa	Sea ice in Antarctica
ColAFP	*Colwellia sp. SLW05*	3.8 [0.14 mM]	26 kDa	Sea ice in Antarctica

Abbreviations used in this table: wf, winter flounder; ss, shorthorn sculpin; Ca^{2+} -in, Ca^{2+} -independent; Ca^{2+} -de, Ca^{2+} -dependent.[22,30,39,41,43,57,59,67,78,94,100–103]

Chapter 2

Ice Recrystallization Inhibition Activities of Different AFPs

2.1 Abstract:

Ice recrystallization corresponds to a phenomenon where large ice crystals are formed at the expense of small ice crystals. Antifreeze proteins (AFPs) are able to arrest such phenomenon at micro molar level concentration. Here ice recrystallization inhibition (IRI) efficiency was measured for the wild-type AFPI-III, a defective AFPIII isoform and a fungal AFP isoform. We monitored specific ice grains exhibiting only uniform growth, for which maximum Feret diameter was measured. The slope of a plot representing the cube of an ice grain`s radius (r^3) against time gave the recrystallization rate (k). A significant difference in k per molar concentration between the analyzed AFPs were observed in the data.

Outlines:

In this chapter the author described the contents of an unpublished manuscript entitled “Ice recrystallization is strongly inhibited when antifreeze proteins bind to multiple ice planes ” by Anika T. Rahman, Tatsuya Arai, Akari Yamauchi, Ai, Miura, Hidemasa Kondo, Yasushi Ohyama, and Sakae Tsuda. The authors contributions are A.T.R., Y.O. and S.T. designed research. A.T.R., T.A., A.Y., A.M., H.K., and Y.O. performed research. A.T.R and S.T. wrote the paper. Here, mass purification of analyzed proteins and their ice recrystallization inhibition efficiencies at different concentrations have been reported.

2.2 Introduction:

The phenomenon of ice recrystallization (IR) has been expansively studied. It can occur during the freezing, storage and thawing cycles of cryopreservation where cells, tissues and other biological materials are stored at very low sub-zero temperatures. The detrimental effect of ice recrystallization is mainly attributed to the thawing phase of cryopreservation due to its fastest rate of occurrence[104].

Ice exits as hexagonal ice lattice unit (I_h) below 0 °C and atmospheric pressure. The unit has a regular crystalline structure with an ordered arrangement of intermolecular hydrogen bonds between water molecules where a single oxygen atom is hydrogen bonded to two hydrogen atoms. Ice lattice unit is characterized by four axes (a_1, a_2, a_3, and c). Eight faces are present on the surface of each unit among which two faces are normal to c-axis named basal planes. The other six faces are prism faces. Water cannot move automatically between ice lattice and bulk water due to presence of a thin semi-ordered layer named quasi-liquid layer (QLL). The layer is about 10-15 Å thick which varies on a temperature dependent manner. At -0.03 °C, the thickness is about 15 nm which decreases to 0.3 nm at -10 °C. The 15 nm thickness is about the forty monolayers of water whereas 0.3 nm represents about of one monolayer of ice. The characteristics like density profile, translational or orientational order and diffusion constants of water in QLL fluctuate among different ice faces. Studies reported the presence of thicker QLL in prism and basal faces than pyramidal and secondary prism plane[105].

The ice crystals perform their recrystallization processes in different manners including growing uniformly, shrinking by melting or disappearing or merging to become larger ice grains[106,107]. The growing and shrinking type of IR are known as migratory recrystallization. In migratory recrystallization, small ice crystals cannot bind their surface water molecules as firmly as large ice crystals because of higher curvature and thus they possess larger surface free energy. The water molecules on the surface of small crystals tend to migrate to the surface of large ice crystals. The overall process results in growth of large ice crystals and disappearance of small ice crystals[108]. Schematic illustration of each type of recrystallization are shown in figure 2.1.

The Ostwald ripening principle is usually employed to evaluate the recrystallization rate which is represented as follows: $r^3 = r_0^3 + kt$, where r_0 is the radius of an average ice grain size at $t = 0$, and k is the recrystallization rate ($\mu m^3.min^{-1}$)[108].

Antifreeze proteins (AFPs) has the ability to stop recrystallization process[85,109,110]. Despite great studies on ice recrystallization inhibition (IRI) with many AFPs using many tools and softwares, the detailed mechanism of the inhibition is yet to be understood[85–90].

In the present study, a video file was analyzed where uniform growth of 13-15 ice grains were only monitored in different types of AFP solutions. The author describes the ice recrystallization inhibition activities of different AFPI-III, one defective type III AFP isoform and one fungal AFP. The current paper also investigated the ice recrystallization inhibition activities of native AFGP sample (isoform mixture).

2.3 Methods and Materials:

2.3.1 Expression and Purification of AFPs:

The samples of AFPI-III were purified from barfin plaice, longsnout poacher and notched fin-eelpout respectively[69,78,111]. The fishes were caught from Okhotsk coastal area of Hokkaido island in the middle of winter. In 2016, the Nichirei Corporation prepared their muscle homogenates (6-19-20 Tsukijim Chuo-ku, Tokyo 104-8402, Japan). The homogenates were further utilized for purification. The recombinant isoform of AFPIII was mutated in its 20th position with Leu. The recombinant fungal AFP isoform was prepared using standard overlap extension PCR methodologies. *Escherichia coli* BL21 (DE3) containing expression vector was cultured in Luria-Bertani medium and the products were purified using cation exchange chromatography (Econo-Pac High S column, Bio-Rad, USA) with a linear gradient of NaCl (0-0.5 M) using 10 mM acidic buffer (pH 3.0). The purified AFP samples were dialyzed against milliQ and lyophilized.

The native AFGP sample (isoform mixture) was purchased from NICHIREI Corporation, Japan. But there are some problems like there are no information about the source material

(probably a kind of cod species) and about an averaged molecular weight of that sample: native AFGP is a mixture of various length of the isoforms. Here, we assumed an averaged molecular weight of 15 kDa for the AFGP sample by considering that Antarctic CodAFGP`s molecular weight distribution from 2.2 to 36 kDa.

2.3.2 IRI Assay:

2.3.2.1 Development of Ice Crystals:

Ice recrystallization inhibition activity experiment was carried out with a photomicroscope system described by Takamichi et al (2007)[82]. The photomicroscope system is composed of a Leica DMLB 100 photomicroscope armed with a Linkam LK600 temperature controller and a CCD camera (figure 2.2). Ice crystals were developed according to modified "Sucrose Sandwich splat assay" described by Smallwood et al (1999)[112] .The assay involved rapidly cooling a sample droplet (1µL) of AFP analyte to -40 °C at a rate of 20 °C/min to induce nucleation event followed by heating to -6 °C at a rate of 10 °C/min to obtain a polycrystalline ice sample. Each sample was then kept at this temperature to perform the recrystallization process (figure 2.3).

The activity was determined quantitatively at different concentration of AFPs to determine the threshold concentration below which ice crystal growth is visible in photomicroscope videos taken with 10X magnification during a specific time interval. Images of 20, 25, 30, 35 and 40 minutes were collected from the video and were considered as images of 0, 5, 10, 15 and 20 minutes respectively. Besides, the whole video was analyzed so that the recrystallization processes of each and individual ice cry could be analyzed.

2.3.2.2 Image Analysis:

The images obtained during annealing period with the CCD camera of Leica DMLB 100 with 10X magnification of objective lens were analyzed using ImageJ software. All the images were first converted to an 8-bit type and a scale bar was calibrated each time by pixel

units. After adjusting the threshold value, Feret diameters of ice crystals in each image were measured (figure 2.4).

2.3.2.3 Evaluation of Ice Recrystallization Rate:

The ice crystals were not always round in shape but were modified into squares and polygonals. Most of the ice crystals in the reference solution (40% solution) exhibit the circularity above 0.8. We therefore set the circularity of ice grains in all solutions to be selected at 0.8-1.0. Image-J software (http://imagej-nih.gov/ij/) was employed for this analysis, which automatically extracts the area (A) and perimeter (P) of the ice grains to calculate their circularity ($R= 4\pi AP^{-2}$) where R=1 implies perfect roundness. The radius (r) was calculated as the half-length of the longest distance of the ice grains or the maximum Feret diameter. A total of 13–15 ice grains were picked out from the video, whose radii were measured at 20, 25, 30, 35, and 40 min. The measurement was performed for 3–5 subsets of the 13–15 ice grains. Videos were recorded for all AFP samples at various concentrations. We only used growing type of recrystallization process for evaluating the recrystallization process.

The obtained mean radius of each sample along a specific time interval was utilized in theory of Lifshitz, Slyozov andd Wagner (LSW theory) to calculate IRI rate.The theory states that the diffusion of water molecules is mainly occuring in the ice recrystallization process and the temporal increase in the mean crystal radius r according to LSW theory is as follows:

$r^3 = r_o^3 + k_d t$

Where $r_\circ$ is the initial mean radius at time t=0 min and k_d corresponds to the observed rate of recrystallization [113]. This equation is appropriate in our sandwich IRI assay with 40% sucrose where migratory recrysalliation or Ostwald ripening dominates [89]. Less than 50% standard deviation in each recrystallization rate value were considered to compare k_d values among different AFPs in different concentration.

The mean values of r^3 in each collected image were plotted against its corresponding time and the slope of best fitted line was considered as ice recrystallization rate. The set of k values were later fitted in sigmoidal curves.

2.3.3 Evaluation of Ice Volume Fraction:

A question arises when we consider the growth of only 13-15 ice crystals in evaluating average ice recrystallization rate that whether our selected 13-15 ice crystals are the statistically valid extraction or simply "statistical sample". The examination of time dependence of the ice volume fraction of our monitored 13-15 ice crystals was done by dividing the total area of 13-15 ice crystals by total area occupied by all ice crystals in every image.

2.4 Results:

2.4.1 Evaluated Ice Recrystallization Inhibition Rates of AFPs:

Previous methods measured average ice grain size from photomicroscope images and determined the minimum AFP concentration to halt the ice recrystallization process[89,113]. It was considered as "IRI endpoint"[114–116]. Our video method determined the IRI endpoint from the time-interval snapshots of the ice grains. The images presented in figure 2.5B compare the sizes of ice grains for 1.5 μM solutions of the five AFP samples during a 20 min annealing period at -6 °C. The larger ice grains were shown in 40% sucrose, AFPI, AFPIII and A20L solutions. But the sizes of ice grain did not change during the annealing period in Tis8 and AFPII solution. Addition of more AFPs in AFPI solution makes the image of AFPI like Tis8 and AFPII solution.

Figure 2.6 shows time-dependence data of the r^3 values (μm^3) of ice grains examined at 1.5, 3.0, 6.0, 8.0 and 10.0 μM solutions of AFPI. The plot also presents the time-dependence data of 40% sucrose. The r^3 values increased linearly with time and the obtained slopes were used to evaluate recrystallization rate. Similar types of plots were also obtainable from the other analyzed AFPs.

Fitting of a sigmoidal curve of the formula[113] to a set of the *k* values determined at different AFP concentrations was employed to examine the ice recrystallization kinetics (figure 2.7). The inflection point of the obtained semi-log plot gives the concentration of AFP (C_i) at which it is assumed to occur a turnover from diffusion-limited growth to liquid-to-ice-transfer-limited growth due to AFP binding on ice surface. All the *k* values obtained from different AFPs at varied concentrations were fitted in S-shaped curves in the semi-log plot.

The obtained C_i values are as follows: 0.27 μM (Tis8), 0.60 μM (AFPII), 3.00 μM (AFPIII), 4.69 μM (AFPI) and 7.69 μM (A20L). The C_i value for the native AFGP sample was estimated 0.06 μM (figure 2.8).

We also determined the IRI endpoint which is an approximate AFP concentration when *k* becomes zero. The analyzed AFPs gave following approximate IRI endpoint: 0.7 μM (Tis8), 11.0 μM (AFPI), 1.1 μM (AFPII), 8.6 μM (AFPIII) and 12 μM (A20L). The approximate IRI endpoint was found 0.4 μM for the native AFGP sample.

2.4.2 Ice Volume Fraction of AFP Solutions:

Fig. 2.9 presents the plots where the fractions of both reference (40% sucrose) and AFPI (bpAFP) at different concentrations (ex. 1.5 and 3.0 μM) are constant with time (*t*) which indicates that our selected ice crystals are neither local or special, representing the whole system and can be regarded as the statistical sample.

Here, we assumed a constant thickness of the sample film in the examined region and a cylindrical shape of the crystals between the lower and upper coverslip.

2.5 Discussion:

Different methods (splat cooling, sucrose sandwich splat assay, capillary) were reported for assaying the recrystallization. All used different concentrations of colligative additives (e.g., salts, sucrose) and annealing temperatures. The first analysis of IRI activity was done by Knight using a splat cooling assay. The assay implicates the dropping of analyte (AFPs) dissolved in PBS onto an aluminium block (-78°C) and successively transferring the resultant

ice wafer to a microscope stage maintaining -8°C to perform ice recrystallization process[85]. Convenient substitutes were proposed afterwards wherein AFP samples are sandwiched between coverslips to make ice crystals by rapid freezing (sucrose sandwich splat assay) or freezing and annealing an AFP sample kept inside 10 µL glass capillary(capillary assay)[112,86] . However all these proposed methods can only provide semi-quantitative result by showing IRI endpoint where no IRI activity exists.

IRI activity was measured also quantitatively by Jackman using domain recognition software to measure areas of 10 largest ice crystals after the annealing period[88]. Though, the method is associated with lack of reproducibility and high throughput measurement. Development of methods involving measuring average radius of ice crystals using Feret diameter or circle hogue transformation included all ice crystal images in calculation instead of 10 largest ice crystals to obtain a statistically significant result[67,113]. Although the methods do not allow for controlling ice crystal numbers.

Here, a method of measuring IRI rate is employed from micrographs taken during an IRI experiment by reshaping conventional "Sucrose Sandwich Splat Assay" and using open source ImageJ software. The process involves the measurement of 13—15 growing ice crystals with a circularity of 0.8 or above during a specific time interval. Feret diameter which corresponds to the longest distance between any two points along the selection boundary is used as a parameter to calculate the radii of ice crystals. The average radius of same 13—15 ice crystals in each image was latterly used in evaluating IRI rate. The effect of initial average ice crystal radius of AFPI samples at different concentrations suggested that as initial average radius becomes smaller, the slope of the straight line obtained from r^3 vs. t plot become mild as shown in figure 2.6.

The proposed method of the IRI micrographs chases specific ice crystals along the experimental course, which provides significant accuracy to quantitative evaluation of ice recrystallization kinetics. Moreover, the remodelled method put some criteria to evaluate IRI. Firstly, it analyzes the ice crystals having circularity of 0.8 or above as most of the ice crystals in the reference solution (40% sucrose) exhibit the circularity above 0.8. Secondly,

it analyzes the same 13 to 15 ice crystals in all images captured between 20 and 40 minutes of each sample which is giving opportunity to control the number of ice crystal along the experiment time. The method keeps the sandard deviations of different rate constants always around 50%.

According to our reshaped method of measuring C_i, we ranked the five analyzed AFPs as follows: Tis8 (0.27 µM) > AFPII (0.60 µM) > AFPIII (3.0 µM) > AFPI (4.69 µM) > A20L (7.69 µM). The, Tis8 is the most IRI active the value of C_i (the AFP concentration at which it is assumed to occurrence of turnover from diffusion-limited growth to liquid-to-ice-transfer-limited growth induced by AFP binding on ice surface).

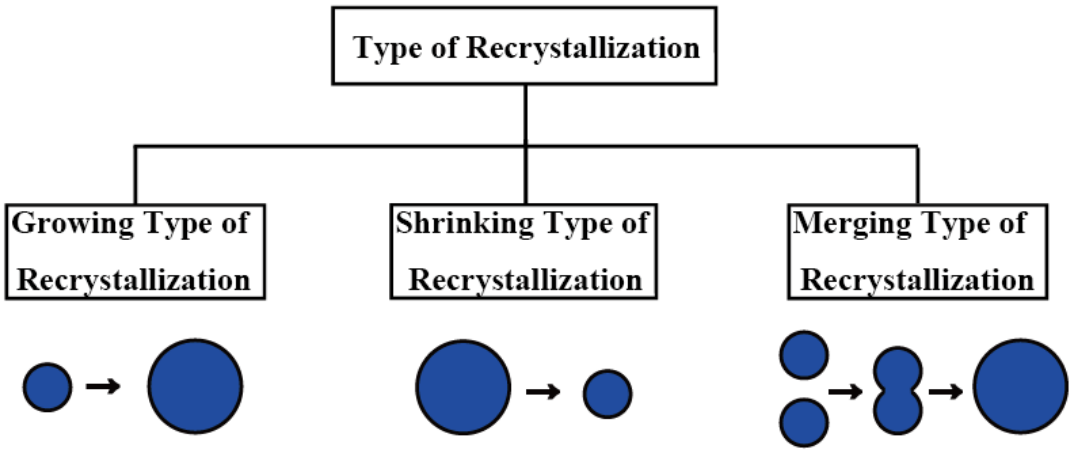

Figure 2.1: Schematic representation of three types of ice recrystallization processes.

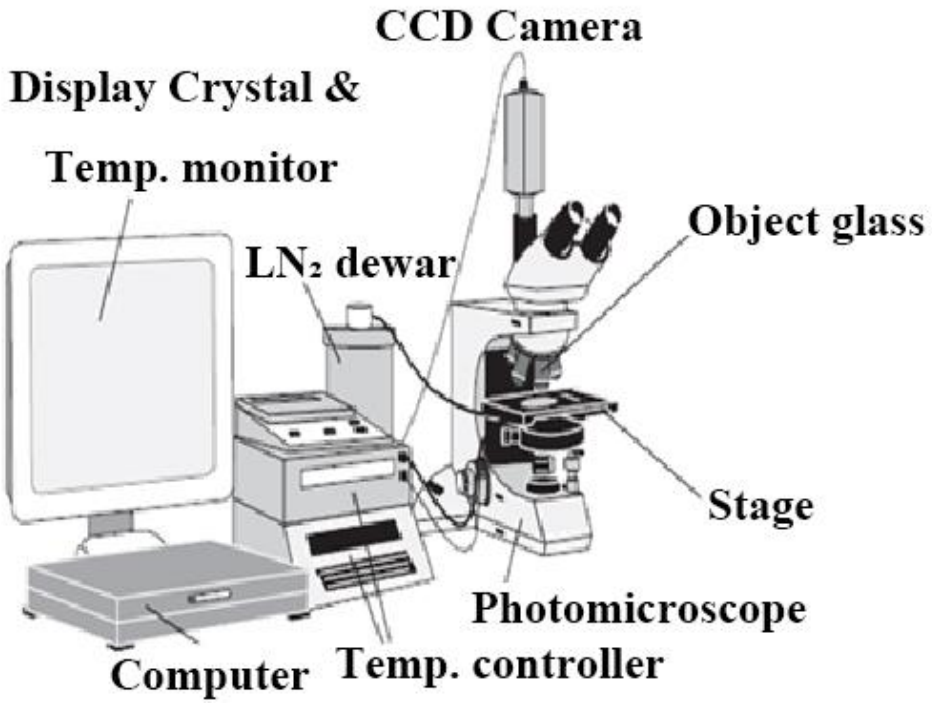

Figure 2.2: A photomicroscope equipped with a temperature controller for measurement of IRI rate.

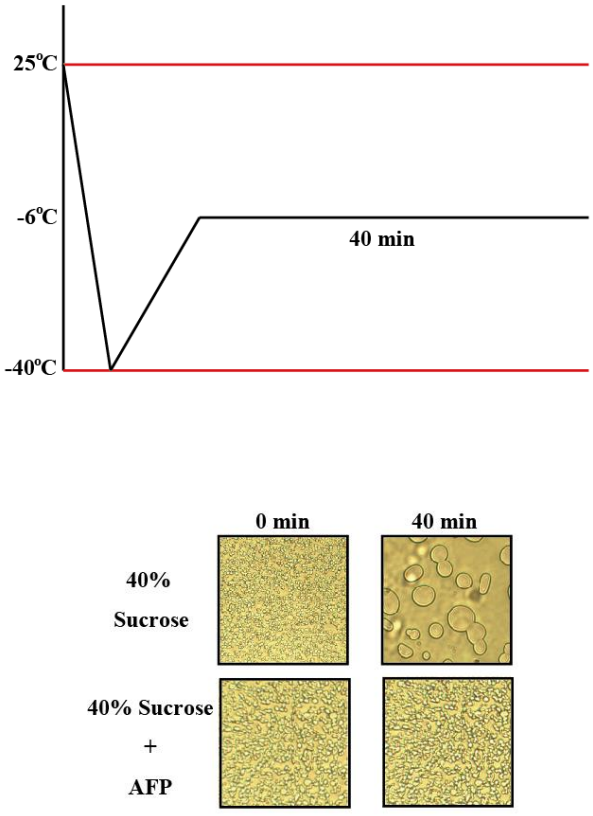

Figure 2.3: Illustration of procedure for measuring IRI rates.

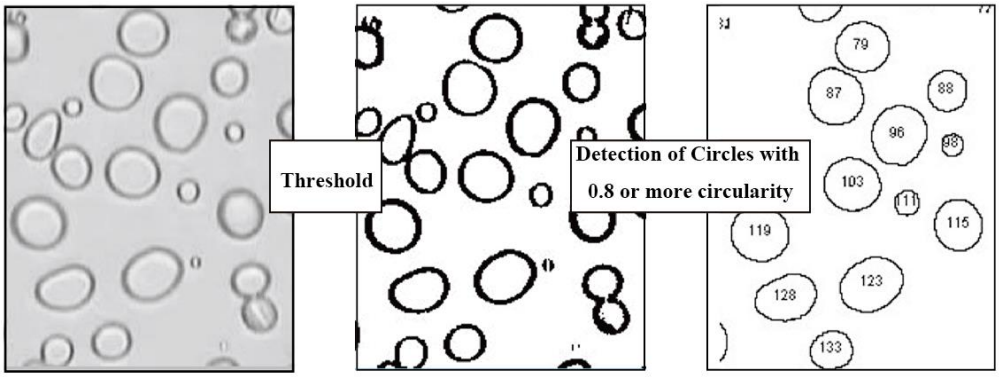

Figure 2.4: Overview of the image analysis process employing feret diameters to detect ice crystals.

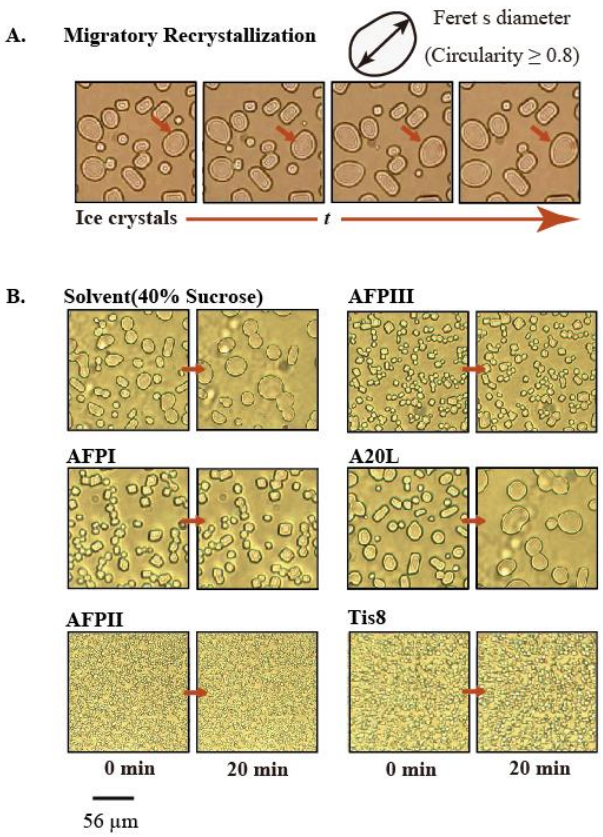

Figure 2.5: Photomicroscope snapshots of ice grains picked up from 40 min videos that recorded the ice recrystallization process.

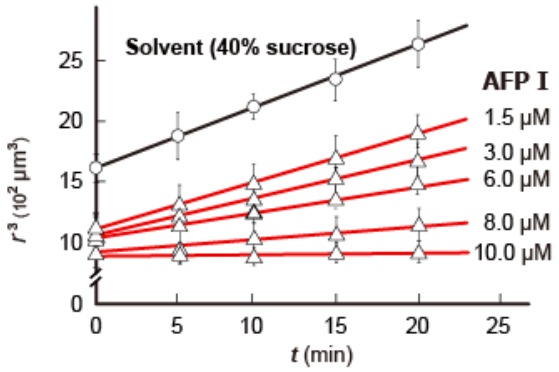

Figure 2.6: Time-dependence of the ice crystal radius cubed (r^3) of AFPI at different concentrations.

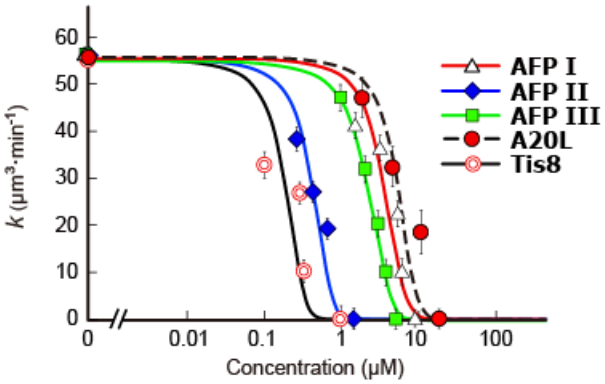

Figure 2.7: The concentration dependence of recrystallization rates (k) ($\mu m^3.min^{-1}$) for the five AFP samples (AFPI-III, A20L and Tis8).

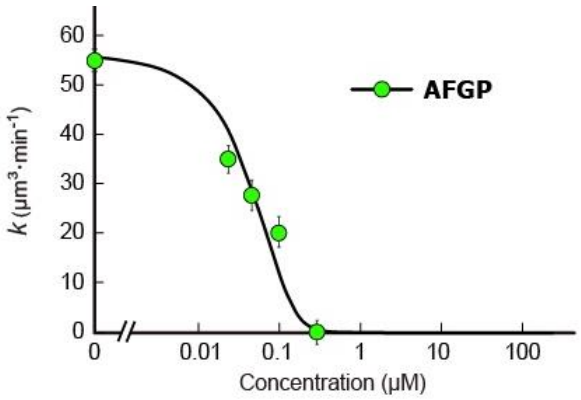

Figure 2.8: The concentration dependence of recrystallization rates (*k*) (μm^3.min^{-1}) for the AFGP sample.

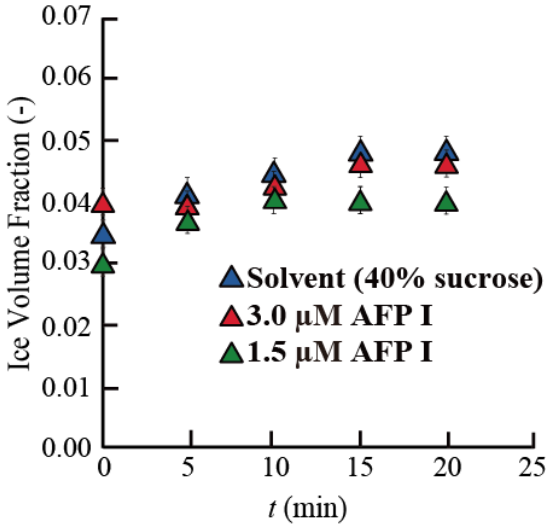

Figure 2.9: Time-dependence of the ice volume fraction during the IRI experiments. Ice volume fraction defined by ∑ area of 13-15 ice crystals / ∑ area of all ice crystals was evaluated for a reference solution (40w/w% sucrose, blue triangle) as well as the AFPI (BpAFP) solution at the concentrations of 3.0 (red) and 1.5 µM (green).

Chapter 3

Ice Plane Specificities and TH Activity of Different AFPs

3.1 Abstract:

Antifreeze proteins (AFPs) specifically binds onto the embryonic ice crystal surfaces to inhibit their growth. The effectiveness of AFPs` can be evaluated quantitatively by measuring thermal hysteresis (TH) activity. The activity arises from the depression of freezing temperature in a non-colligative manner upon AFP binding. In addition, a technique named fluorescence based ice-plane affinity (FIPA) can be employed to detect ice-binding activity of AFPs` qualitatively. Here, determination of TH activity as well as development of FIPA images were done for type I-III, a defective type III isoform and fungal AFP. The resultant values and images were compared with the ice recrystallization inhibition (IRI) efficiency of the analyzed AFPs. By combining all the results, it could be said that ice recrystallization is strongly inhibited when antifreeze proteins bind to multiple ice planes.

Outlines:

In this chapter the author described the contents of an unpublished manuscript entitled "Ice recrystallization is strongly inhibited when antifreeze proteins bind to multiple ice planes" by Anika T. Rahman, Tatsuya Arai, Akari Yamauchi, Ai, Miura, Hidemasa Kondo, Yasushi Ohyama, and Sakae Tsuda. The authors contributions are A.T.R., Y.O. and S.T. designed research. A.T.R., T.A., A.Y., A.M., H.K., and Y.O. performed research. A.T.R and S.T. wrote the paper. Here, relation of ice recrystallization inhibition efficiency of different AFPs with their ice binding properties have been reported.

3.2 Introduction:

A wide range of organisms is inhabiting sub-zero temperature by expressing of antifreeze proteins (AFPs) which modulate the effect of ice on their lives [23, 117,118]. AFPs adsorb to the surface of seed ice crystals to stop their growth[119]. When an AFP species binds to specific ice crystal plane(s), a curved ice front is created on that plane between the bound AFPs due to Gibbs-Thomson effect[81;119]. The curved ice- front becomes thermodynamically unfavorable for further ice growth [11]. This leads to depression of the non-equilibrium freezing temperature (T_f) and slightly elevation of the equilibrium melting temperature (T_m) [120]. The resultant difference between T_m and T_f is considered as thermal hysteresis (TH) activity of a specific type of protein[121].

The unit structure of an ice crystal is hexagonal (I_h). It has three equivalent *a*-axes (a_1-a_3) perpendicular to the *c*-axis in which ice crystal planes are represented by Miller-Bravais indices. The top and bottom planes are basal planes denoted by {0001}, which are normal to the *c*-axis. The six equivalent side faces are known as primary prism planes {10-10}. The pyramidal plane is indicated by {20-21} which is a sloped slice inclined by 14.9 to the c-axis.

Surface adsorption of an AFP is specific for one or more planes of ice. The moderately active AFPs direct ice crystal growth along the *c*-axis when TH is exceeded whereas hyperactive AFPs allows growth along *a*-axes. Both types of AFPs show concentration dependency in exhibiting TH activity. The affinity towards specific ice planes played an important role in earlier work in exhibiting specific type of TH values in each category of AFP[65].

The ice binding property of an AFP can be detected directly, albeit in a qualitative fashion through fluorescent based ice-plane affinity (FIPA) technique[110]. Here, AFPs are fluorescently labeled with a chimeric tag, such as green fluorescent protein (GFP) or with fluorescent dye covalently bound to the AFP. The fluorescently labeled AFP solution is then slowly incorporated into a single ice crystal hemisphere of 2-3 cm in diameter. Each type of AFP shows specific pattern on ice hemisphere under UV light after growth of the hemisphere into a certain size.

Illumination of six equally distant ellipses on the equator denotes AFP binding on six equivalent prism planes of a single ice crystal. Additionally, illumination of six ellipses on the mid-latitude indicates AFP binding on six equivalent pyramidal planes. Entire ice hemisphere illumination implies the AFP binding on multiple ice plane [122,99,97].

The type I AFP from winter flounder binds to the 20-21 pyramidal planes whereas type III AFPs binds both primary and pyramidal plane. A hyperactive AFP from spruce budworm binds simultaneously primary and basal planes. Another hyperactive AFP named MpAFP binds multiple ice plane which is indicated by the whole ice surface coverage of single ice crystal. A hypothesis suggested basal plane binding of AFP together with the other planes are reason for 10-fold higher activity than moderately active AFPs [122].

The tertiary structure of AFPs determines the mechanism of ice-binding. For example, AFPI has three repeats of an 11-residue consensus sequence (Thr-X_{10}, where X is mostly Ala) which makes an α–helical[92]. Four OH-groups of AFPI protrudes on one side of this molecule at intervals of 16.5 Å. The consecutive Ala residues forms ice-binding site (IBS) which binds to pyramidal plane of ice complimentarily where the oxygen atom spacing is 16.7 Å. Specific type of IBS is formed on each type of AFP structure, which has characteristic planer hydrophobic surface that incorporates several polar groups[22].

The present chapter focused on determining TH activities and developing FIPA patterns of type I-III AFP, a defective type III isoform and one fungal AFP to clearly demonstrate the reasons of their different ice recrystallization inhibition (IRI) efficiency described in previous chapter. The TH activity of AFGP sample was also brought in discussion for comparison. Additionally, this chapter focused on evaluating "ice binding site" (IBS) of each AFP and analyzing "ice shaping activity" of different AFPs during recrystallization experiment.

3.3 Materials and Methods:

3.3.1 TH Activity Measurement:

TH activity was measured with a LEICA DMLB photomicroscope (Leica Microsystems,Wetzlar, Germany) equipped with a Linkam THMS 600 temperture controllar

(Linkam Scientific Instruments Ltd, Tadworth, Surrey, UK). Briefly, the method involved freezing an AFP sample of 0.8 µL in the photomicroscope apparatus and melting back to prepare a single seed ice crystal. The AFP sample was then cooled at a rate of 0.1 °C.min^{-1} until a rapid growth of ice crystal was observed. The temperature at which rapid growth of ice crystal occurred was considered as freezing point (figure 3.1). The mesurements of *Tm* and *Tf* values were repeated three times for each type of concentration and averaged values were considered as the TH activity. The crystallographic symmetry determined the directions of the ice crystals prepared in AFP solutions. The bursting towards two-fold symmetry indicates a crystal growth along the c-axis and and towards six-fold symmetry indicates a crystal growth towards directions normal to c-axis. The fish AFP samples were prepared by dissolving required amount of AFP in millQ and 25mM ammonium bicarbonate (pH 7.9) was used in dissolving the fungal AFP (Tis8). The AFGP sample was also dissolved in milliQ for TH measurement.

3.3.2 Fluorescence—Based Ice Plane Affinity (FIPA) Analysis:

Single ice crystal was prepared using the procedure developed by Garnham et al[76]. Briefly, degassed ultra pure water (MilliQ) was poured onto a stainless steel pan containing PVC pipes with a tiny notch on the bottom that floats in a temperature-controlled bath and supercooled at -0.5 °C. An ice particle was then added to the supercooled water for seeding. The ice needle entered into the PVC pipes through tiny notch and formed single ice crystal in each of PVC pipe. The quality of each single ice crystal was checked through a polarizing filter.

The fluorescent—labeled AFPs were prepared by reacting each AFP in 100 mM $NaHCO_3$ pH 8.5 with equivalent amount of flurescent detergent tetra—methyl—rhodamine [5(6)—TAMRA—X, SE;Thermo Fisher scientific]. The solution was allowed to mix in a tube rotator for 3 h at room temperature. The unreacted compounds were removed by dialyzing against distilled water.

The FIPA analysis was performed for the AFP samples according to the previously described methods[77,123]. The method involved attaching a single ice crystal hemisphere of 2.5 cm in diameter to a brass cold-finger cooled at -0.5 °C and immersing it in a fluorescently labeled AFP solution in an insulated cup. The temperature of the cold—finger was immediately lowered to -5 °C and a hemisphere shaped ice crystal was allowed to grown for 4—5 h. The detailed illustration of FIPA experiment is shown in figure 3.2.

After growing to a desired size (5 cm), the hemisphere was detached, wiped with a disposable tissue to remove nonspecifically bound mterials. The ice crystal was illuminated under UV light and photographed at -1 °C.

Different types of AFPs shows different pattern on ice crystal hemisphere. The relationship between the hexagonal ice unit and the FIPA pattern is shown figure 3.3, for which the ice hemisphere was attaced to cooled probe in two different ways; one is to attaching the ice hemisphere directing its *c*-axis downward (figure 3.3, a2, b2, c2 and d2) and another is to direct the 1st prism plane downward (figure 3.3, a3, b3, c3 and d3). When one AFP specifically target 1st prism plane, the patterns in figure 3.3 b2 (image obtained along the *c*-axis) or b3 (image obtained normal to the *c*-axis). Patterns like c2 and c3, and those like d2 and d3 are formed when secondary prism planes and pyramidal planes are targetted by AFPs respectively. Superposition of different patterns are seen when AFPs simultaneously bind multiple ice planes.

In the current study, FIPA pattern of five AFPs were observed on a single ice crystal hemisphere after soaking it in a 0.1 mg.ml^{-1}.

3.3.3 Evaluation of Ice Binding Site (IBS):

The approximate size of putative IBS (Å^2) for each AFP sample was evaluated using accessible surface area occupied by putative ice binding residues whose summation was considered as the area of IBS for each AFP structure[78,100,111,123–125]. The AreaIMOL program of CCP4 software package[126] was used for this evaluation.

3.4 Results:

3.4.1 TH Activities of AFPs:

TH activities of four AFPs were evaluated as a function of the protein concentration. The results are shown in figure 3.4. The AFPI showed a TH activity of ~0.25 °C at 1.3 mM concentration. The AFPII and AFPIII possessed 0.44 °C and 0.29 °C TH activities at 0.22 mM concentration respectively. The Tis8 presented a TH activity of 0.6°C at 0.12 mM concentration (figure 3.4). So, it is the most active AFP among the analyzed proteins. The A20L could not show any TH value. Ordering AFPs based on TH activity from the most to the least active gives Tis8 > AFPII > AFPIII > AFPI. The AFGP sample showed 0.5 °C TH at 1.4 mM concentration which is demonstrating this sample as moderate active (figure 3.5).

3.4.2 Proteins Bound Differently to Ice Crystal Hemisphere:

Figure 3.6 compares the FIPA patterns between the AFP samples. The images a1 and a2 are the photographs of ice hemispheres grown in presence of AFPI sample. The image a3 is depicting the schematic illustration of a2. The a2 image is formed due to targeting of AFPI sample to secondary prism planes and pyramidal planes. The AFPII targeted multiple ice planes except the basal planes (figure 3.6, b1-b3) while the AFPIII showed its affinity towards limited regions of the 1st prism- and pyramidal planes (figure 3.6, c1-c3). The A20L bound to a limited area in the pyramidal planes (figure 3.6, d1-d3), which is the smallest among the analyzed AFP samples. The ice hemisphere was found entirely illuminated in the presence of Tis8 sample. So the Tis8 binds whole ice crystal planes in a single ice hemisphere.

The AFP samples can be ranked on the following sequence if they are arranged in decreasing order of adsorption area: Tis8 > AFPII > AFPIII > AFPI > A20L.

3.4.3 Sizes of Ice Binding Site (IBS):

The table 3.1, 3.2, 3.3, 3.4 and 3.5 show the putative ice binding residues responsible for making “ice binding site” (IBS) on each type of AFP (AFPI-III, A20L and Tis8). The size order was Tis8 (1544 Å^2) > AFPII (1149 Å^2) > AFPIII (820 Å^2) > A20L (696 Å^2) > AFPI (564 Å^2).

The figure 3.7 is showing the structural models created with Pymol of the studied AFP samples. On each type of structural model, a square is drawn which is depicting the ice-binding regions, though it is not perfectly formed for A20L.

3.4.4 Ice Shaping Activity:

Ice crystals in pure sucrose solutions remained circular throughout the experiment while those with AFPI-III or A20L adopted a hexagonal crystal habitus after having a certain concentration. It occurred because some inhibitors like AFPs adopt a hexagonal crystal habitus. Specific moieties of the AFPs form hydrogen bonds that match the pattern of O atoms in particular ice face[7,81]. The AFP adsorbed faces grow at a much slower rate and hence ice crystals presents a crystal habitus that is very specific for a particular type of AFP. Some ice shaping activities of analyzed AFPs are depicted in figure 3.8B. The AFPI started showing hexagonal crystal plate like structure at 1.5 µM concentration whereas AFPII showed the same crystal habitus at 0.8 µM concentration. The hexagonal crystal habitus for AFPIII was found at 1.4 µM. The A20L needed 5.6 µM to show its ice shaping activity. The Tis8 showed no ice shaping activity.

3.5 Discussion:

The present study evaluated TH values of AFPI-III, A20L and Tis8 by measuring the growth-initiation temperature (T_f) and the melting temperature (T_m) of a single ice crystal, where the crystal size (1.5 µm) and cooling rate (0.1 ℃.min^{-1}) were adjusted throughout the experiments. The Tis8 AFP sample (a hyperactive AFP) showed highest TH values (2.2 ℃). The AFPII and AFPIII samples gave 1.1 ℃ and 0.9 ℃ TH values. The A20L could not prevent ice growth which resulted in failing to get a TH value for the AFP sample. The AFGP sample exhibited moderate TH activity. Although the highest IRI efficiency was observed in Tis8 AFP sample, it could not show any specific relation with the other analyzed AFP samples regarding to its TH values. Previous work also could not show any correlation between the TH and IRI[67,89].

We know that the secondary prism plane provides the most favourable and fastest growing ice lattice direction compare to other primary prism pane or pyramidal plane due to the formation of cooperative hydrogen bond to the ice lattice by chains or networks of water molecules[10,93]. Primary prism plane offers the slower growing direction than this plane as only pairs of water molecules can attach with ice lattice due to possesion of one hydrogen bond per two water molecules. The slowest growing ice lattice direction is basal plane as 2D nucleation is needed here on the molecularly smooth basal plane to start the recrystallization process [67].

Comparing all these facts, the reason of strongest IRI efficiency of Tis8 may be no availability of ice planes to grow in presence of this AFP. The next IRI efficient compound was found AFPII as it is providing only basal plane to grow. The AFPIII is showing higher IRI efficiency than AFPI despite the AFPIII is allowing the gowth of secondary prism plane as AFPI. The most likely reason behind this might be the amount of coverage on ice crystal planes by these two AFPs. The AFPI might have covered smaller area on ice lattice to inhibit the recrystallization process. It was previously reported that larger inhibitors exhibit a larger adsorption constant because they can bind more strongly to the ice faces due to a larger number of moieties that can form hydrogen bonds. This ultimately leads to an irreversible adsorption process, an phenomenon that is also thought to be the cause for the strong change in thermal hysteresis when measuring from smaller to to larger AFP[113]. Therefore, it is resonable to obtain better IR rates for AFPIII than AFPI as the molecular weight of AFPI is just 3.2 kDa whereas AFPIII possess the molecular weight of 7 kDa. Although the molecular weight of A20L is about 7 kDa, it is showing the least IRI activity among all AFPs. The most likely explanation for the lowest activity of this AFP is that its IBS has least complementarity with ice surface.

The size order of the IBS for the analyzing AFPs was found as follows: Tis8 (1544 $Å^2$) > AFPII (1149 $Å^2$) > AFPIII (820 $Å^2$) > A20L (696 $Å^2$) > AFPI (564 $Å^2$). So, it can again be suggested that larger IBS causes more IRI efficiency ignoring little higher IBS size in A20L than AFPI.

The FIPA data or IBS size of native AFGP sample could not be analyzed. The AFGP sample does not contain any lysine residue which is indispensable for its fluorescent labelling. The native sample had a mixture of isoforms whose molecular weights were widely varied.

A single ice crystal is gradually modified through the AFP binding. Generally, it is arranged by hexagonally arranged waters. The ice crystal forms a disk shape without any AFP. Its six prism planes become visible when AFP adsorbs to the waters that construct the planes which eventually forms a hexagonal plate. Further AFP-adsorptions cause new disks formation on both side of hexagonal plate through two-dimensional ice nucleation theory. The added new disks also turn into hexagonal plate like structures. The repetitions of crystal growth and new disk generation progress which ultimately leads to the construction of the bipyramidal ice crystal[79]. The above flow chart of modified ice crystals in presence of AFP is shown in figure 3.8A.

As mentioned in the result section, the morphology of ice crystals in the presence of AFP needed to exhibit IRI activity was examined in our study. In figure 3.8B, we compared the photomicroscope snapshots of an ice crystal created in each AFP solution at a concentration below its IRI endpoint. The hexagonal plate like structures were observed in AFPI-III and A20L after attaining a certain concentration.

The Tis8 sample formed a disk shaped structure similar to reference solution (40% sucrose). It is already known that hyperactive AFP like Tis8, can bind to multiple ice planes to modify an ice crystal into a rounded lemon shaped morphology[11]. Study of Cheng et al. (2016) reported the formation of hexagonal plate like morphology for 9.0 μM solution of Tis8 during the TH measurement[124] while the IRI activity of the Tis8 sample was found at very low concentration (0.4 μM).

All the above discussion suggests that AFP can shape ice crystals into hexagonal plates even in the presence of 40% sucrose. Additionally, IRI activity can be exerted at extremely low amount of AFP which can form hexagonal plate like structure. The AFP concentration making bipyramidal shaped ice crystal is not necessary for exhibiting IRI activity. It explains

the previous study with 14nM-1.4μM of AFPIII mixed with known cryoprotectants improves viability of cells and tissues after frozen storage[127,128,129]. The excess amount of AFP making bipyramidal shapes might be harmful to various cells due to their sharped edges.

3.6 Conclusion:

We have studied experimentally the ice recrystallization rates in sucrose solution in both the absence and presence of different categories of AFPs. These data were analyzed with a modification to the classical LSW theory which is mainly attributed to the diffusion type of recrystallization. The analysis using this modification shows the ability to measure recrsytallization rate even at 0.06 μM for certain AFP, the concentration which is thought to impossible for measurement of thermal hysteresis activity. Additionally this paper could report a correlationship between ice recrystallization phenomenon and amount of ice plane coverage of AFPs which ultimately indicates that same ice binding sites are responsible to exhibit AFP`s both criteria.

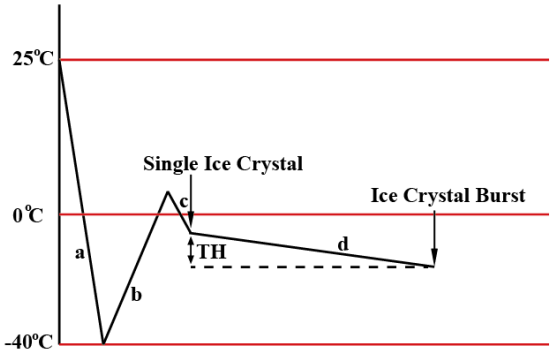

Figure 3.1: Schematic illustration for the measurement of thermal hysteresis activity of AFP samples. (a) A sample droplet immersed in an oil droplet is rapidly cooled to −40 °C to form polycrystalline ice. (b) The sample is slowly melted to form a single ice crystal (c) which is held just below the melting point of the sample. (d) The sample is slowly cooled until a sudden ice crystal burst is observed. The TH is defined as the difference between the melting point of the solution and the temperature at which the ice crystal burst is observed.

Figure 3.2: Schematic illustration of preparation of single ice crystal hemisphere.

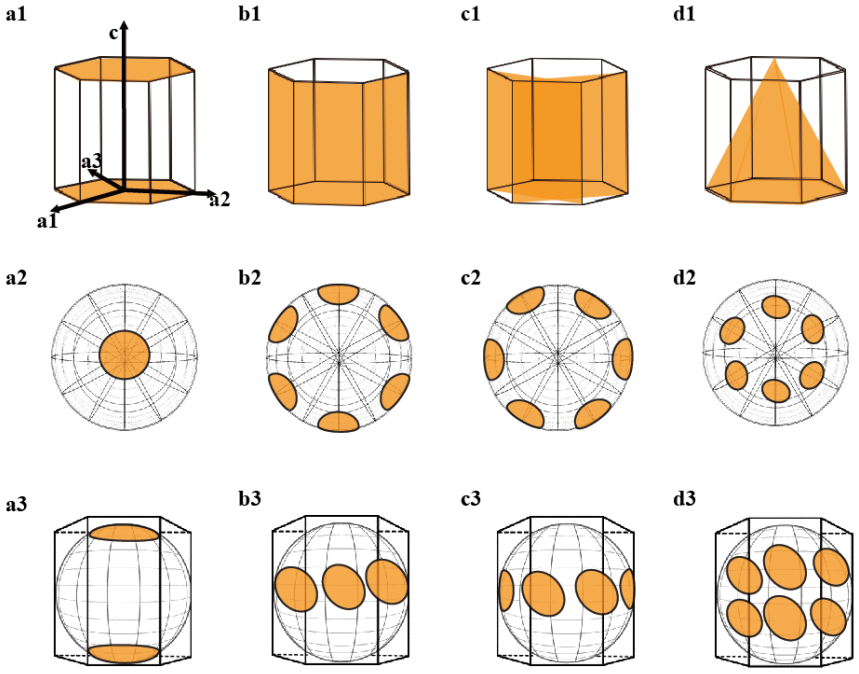

Figure 3.3: Schematic illustration of the ice binding planes of AFPs in a hexagonal ice crystal. The orange colors show the basal planes (a1-a3), first prism planes (b1-b3), secondary prism planes (c1-c3), and pyramidal planes (d1-d3). The crystal graphic *c*- and a_1- a_3 axes are indicated by arrows. Illustrations a2-d2 are the patterns obtained along the *c*-axis. Illustrations a3-d3 are showing the pattern normal to the *c*-axis.

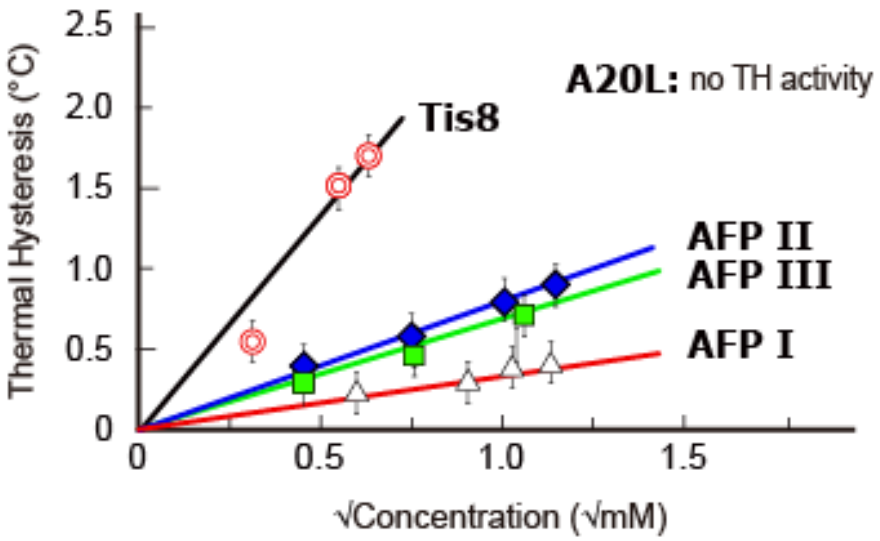

Figure 3.4: Concentration dependence of thermal hysteresis evaluated for the five AFP samples (AFPI-III, A20L and Tis8). The A20L failed to halt the ice crystal growth, for which no TH activity was evaluated.

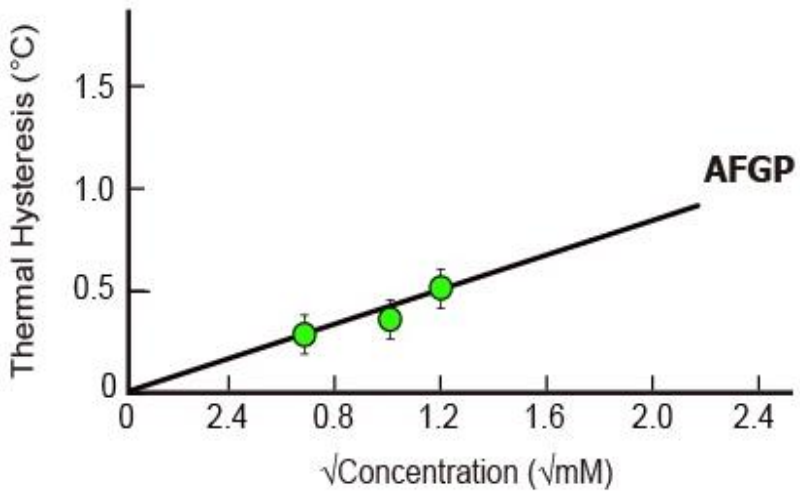

Figure 3.5: Concentration dependence of thermal hysteresis evaluated for the AFGP sample.

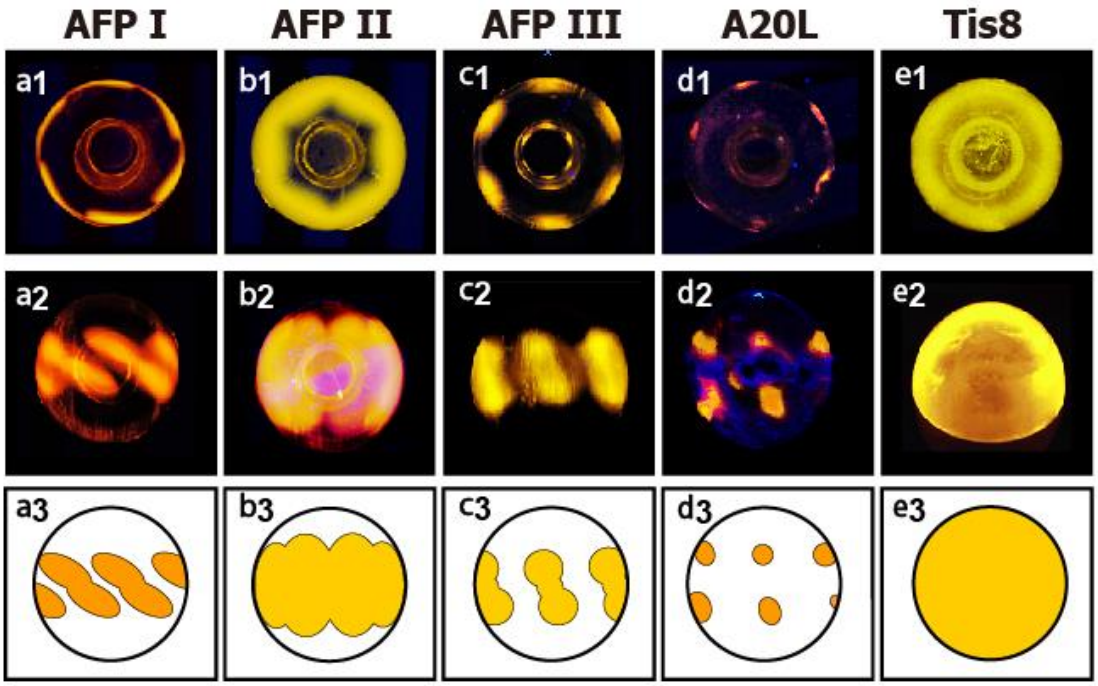

Figure 3.6: Comparison of FIPA pattern between the AFP samples. The images a1-e1 are the pattern along the *c*-axis and a2-e2 are the patterns normal to the *c*-axis. The a3-b3 are showing the schematic illustration of a2-e2.

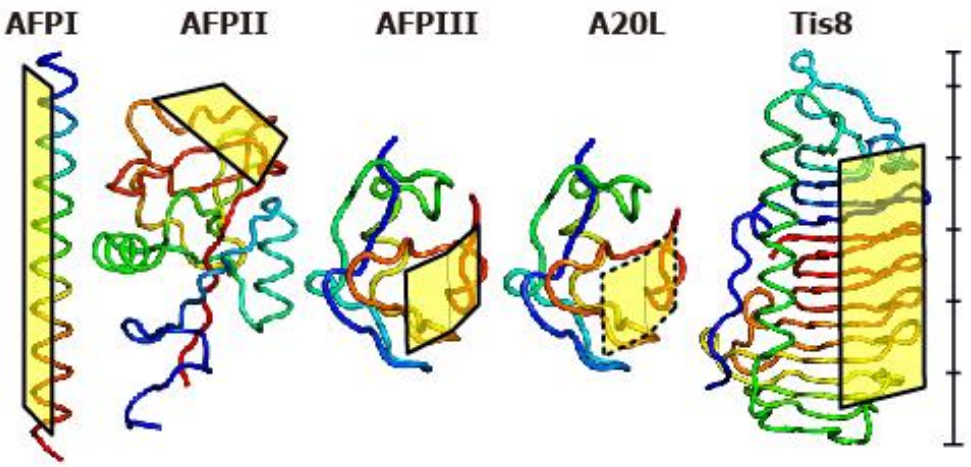

Figure 3.7: Structural models created with Pymol of the AFPs examined in this study[130]. A rod-like α -helical motif (1WFB.pdb) was speculatd for AFPI from barfin plaice. AFPII from longsnout poacher has an elongated globular structure (2ZIB.pdb). AFPIII (5ZXN.pdb) and its defective mutant A20L (5XQV.pdb) from notched-fin eelpout form identical structures except for the 20th residue. Tis8, from snow-mold fungus, forms another globular structures through its β -helical backbone (5b5H.pdb). Squares indicate the ice-binding-regions, through it is not perfectly formed for A20L (hatched square). The structures were adjusted in scale, and a 55 Å scale bar is shown beside Tis8.

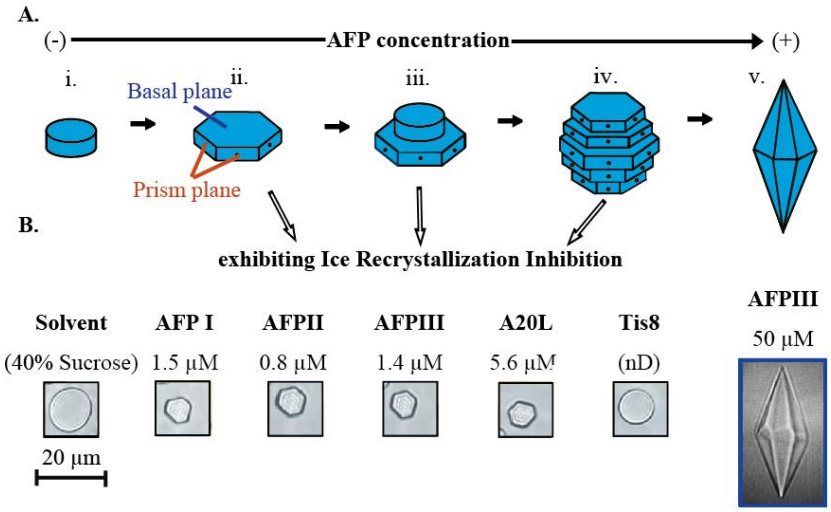

Figure 3.8: Relationship between the morphology of a single ice crystal and AFP concentrations.

Table 3.1: Approximate size of putative IBS constructed in AFPI.

Residue of AFPI	Area (Å^2)	Ratio to calculated GXG value
Thr2	88	0.58
Ala6	59	0.52
Ala10	60	0.53
Thr13	37	0.25
Ala17	15	0.13
Ala21	25	0.22
Thr24	67	0.45
Ala28	36	0.32
Ala32	64	0.55
Thr35	113	0.74
Total	564	

Table 3.2: Approximate size of putative IBS constructed in AFPII.

Residue of AFPII	Area ($Å^2$)	Ratio to calculated GXG value
Ile58	53	0.29
Pro87	107	0.73
Thr88	120	0.76
Lys89	68	0.34
Asn91	83	0.49
Ile93	95	0.54
Ser95	80	0.59
Asp96	48	0.29
Thr102	19	0.13
Ala103	74	0.64
Ala104	40	0.39
Val105	122	0.73
Asp106	87	0.55
Leu112	44	0.26
Ser117	72	0.54
His118	37	0.20
Total	1149	

Table 3.3: Approximate size of putative IBS constructed in AFPIII.

Residue of AFPIII	Area ($Å^2$)	Ratio to calculated GXG value
Gln8	74	0.44
Leu9	73	0.40
Ile12	79	0.43
Asn13	83	0.48
Thr14	35	0.26
Ala15	46	0.42
Thr17	48	0.35
Pro18	48	0.37
Ala19	57	0.48
Met20	21	0.11
Val40	58	0.37
Gly41	54	0.57
Gln43	70	0.37
Lys59	74	0.34
Total	820	

Table 3.4: Approximate size of putative IBS constructed in A20L.

Residue of A20L	Area ($Å^2$)	Ratio to calculated GXG value
Gln8	74	0.43
Leu9	103	0.56
Ile12	88	0.48
Asn13	77	0.45
Thr14	34	0.25
Ala15	44	0.40
Met20	23	0.11
Val40	58	0.37
Gly41	49	0.54
Gln43	72	0.39
Lys59	74	0.34
Total	696	

Table 3.5: Approximate size of putative IBS constructed in Tis8.

Residue of Tis8	Area (Å^2)	Ratio to calculated GXG value	Residue of Tis8	Area (Å^2)	Ratio to calculated GXG value
Pro38	104	0.72	**Gly175**	14	0.19
Ala39	16	0.15	**Ala176**	44	0.38
Phe43	117	0.52	**Val177**	2	0.01
Ser19	18	0.13	**Ser178**	51	0.36
Ala20	47	0.44	**Gln180**	79	0.43
Gly21	6	0.08	**Ala147**	57	0.47
Ser23	40	0.32	**Gly148**	14	0.19
Thr24	13	0.10	**Thr149**	68	0.45
Val25	67	0.44	**Lue150**	10	0.05
Gln210	48	0.23	**Gly151**	25	0.29
Thr211	45	0.30	**Leu152**	6	0.03
Ala212	36	0.32	**Thr123**	87	0.55
Val213	2	0.01	**Ser124**	26	0.25
Ala214	32	0.28	**Pro125**	83	0.58
Leu215	1	0.01	**Total**	1544	
Gln216	54	0.28			
Lys192	90	0.42			
Thr193	48	0.34			
Ala194	40	0.34			
Val195	3	0.02			
Thr196	40	0.28			
Lys198	75	0.37			
Ala174	36	0.30			

Chapter 4

Summary of Ice Recrystallization Efficiencies among Different AFPs

4.1 Abstract:

Ice crystals increase in size within a frozen material through a process called ice recrystallization. Antifreeze proteins (AFPs) can inhibit the process even at sub milli-molar concentrations. Each type of AFP exhibits specific type of efficiency towards the recrystallization process. Although a key determinant of the process is still not understandable. Here, IRI efficiency of different types of AFPs was reviewed to enlighten different aspects of the recrystallization process, which promise to leave their mark on several research fields including structural biology and protein biochemistry.

Outlines:

In this chapter the author described the contents of an unpublished manuscript entitled "Ice recrystallization is strongly inhibited when antifreeze proteins bind to multiple ice planes" by Anika T. Rahman, Tatsuya Arai, Akari Yamauchi, Ai, Miura, Hidemasa Kondo, Yasushi Ohyama, and Sakae Tsuda. The authors contributions are A.T.R., Y.O. and S.T. designed research. A.T.R., T.A., A.Y., A.M., H.K., and Y.O. performed research. A.T.R and S.T. wrote the paper. Here ice recrystallization inhibition efficiency of different AFPs as well as the effects of using different types of solutes during the recrystallization process of those AFPs were discussed.

4.2 Introduction:

The phenomenon called ice recrystallization (IR) is a thermodynamically favorable process in which large ice crystals are formed at the expense of small ice crystals[108]. IR is a regular process in nature and industrial processes during moderate cooling of a partially frozen environment or during temperature fluctuations of frozen substances. It often contributes to the death of cryopreserved cells mainly during storage and thawing[104]. Besides, it has also detrimental effect on quality of frozen foods upon prolonged low temperature storage[108].

4.3 Antifreeze Protein as an Ice Recrystallization Inhibitor:

Biological ice crystal growth modifier "Antifreeze Protein" (AFP) produced by many cold adapted organism adsorbs on ice crystal surface and inhibit its growth hence inhibits the recrystallization process[85,109,110]. The protein does this through prevents the attachment and detachment of water molecule on the ice grains. A better understanding of this ice crystal growth modifier can lead us to development of a nanoparticle with enhanced physical and chemical properties to use in inhibiting recrystallization process effectively[67]. Besides, we will also be able to meet the huge interest in manufacturing inexpensive synthetic ice crystal growth modifier.

Many studies have still been done to correlate the IRI efficacy of antifreeze proteins with its different ice binding properties[8967]. Here, a brief summary of those works which includes the analyzing the correlation of IRI efficacy of various antifreeze proteins with their thermal hysteresis (TH) activity and ice plane affinity are listed. In addition, discussion regarding the effects of different solutes on IRI activity was also carried out in the later part of chapter.

4.4 Correlation between IRI and TH Activities of AFPs`:

The relationship between two ice binding properties of antifreeze proteins, one thermal hysteresis (TH, ability to depress the freezing temperature below the melting point of ice) and another ice recrystallization inhibition (IRI, ability to inhibit the restructuring of ice into

large ice crystals) is still highly debated. Researchers are still unable to establish any distinct correlation between the properties[65,67].

Basically, both TH and IRI properties are executed through binding of AFPs to ice. However, TH activity does not always show proportional relation with the IRI activity.

The comparative study of Yu et al. (2010) between hyperactive insect, bacterial and fish AFPs with the moderately active fish AFPs reported that the TH activity of AFPs are not reflected in the IRI activity. According to the author, the recrystallization experiment is usually performed near melting point where rapid movement of water between grain boundaries is inhibited by AFPs. Ice grains are basically more stable than single, supercooled ice crystals within the TH gap. The overgrowth of an AFP by water molecules at any site on the ice surface will not destabilize ice grains. Both hyperactive and non-hyperactive AFPs are bound and included into ice to similar extent. Therefore, the hyperactivity on the TH value is not seen in the IRI activity[65].

The above study also mentioned that steric mutations on the ice-binding site disrupt the interaction of AFPs with its respective ice binding plane. The A17L and A21L mutations of type I AFP from winter flounder isoform HPLC-6 and the T53Y and T67Y mutations of LpAFP from *Lolium perenne* completely destroys the TH and IRI activity. The steric mutations might reduce the complementarity between the ice surface and AFPs[65].

Although Olijve et al. (2016) described that type III AFP and its T18N mutant showed different TH values instead of possessing same IRI activity[89]. The FfIBP exhibits hyperactivity in TH value with low IRI activity[51].

Our investigated AFPs (AFPI-III, A20L and Tis8 described in second chapter of the dissertation) showed comparable ice recrystallization inhibition activities. The unique concentration (Ci) at which a turnover from diffusion-limited growth to liquid-to-ice-transfer -limited growth occurs was evaluated for each type of AFP[113]. The Ci values were significantly different between the samples, which are 0.27 µM (Tis8), 0.60 µM (AFPII), 3.00 µM (AFPIII), 4.69 µM (AFPI) and 7.69 µM (A20L) respectively. The Ci values for type

I and type III AFP are comparable with the Ci values of 5.8 µM and 5.9 µM for recombinant proteins of AFPI and AFPIII respectively as reported by Olijve et al. (2016)[67].

All our investigated AFPs exhibited TH activity except the A20L sample whose growth inhibition ability was not enough to arrest ice growth. The Tis8 exhibited the strongest IRI, while its difference with the other AFPs was not similar with the difference in TH. So, the overall data is unable to establish any significant correlation between TH and IRI activity.

4.5 Correlation of IRI Activities of AFPs` with Their Ice Plane Affinity:

Fluorescent tagging experiments concluded that high TH activity of specific AFP is due its affinity towards the prism and basal plane[67]. The AFP with moderate TH activity has no basal plane affinity[65].

A complete arrest of ice growth requires a sufficiently high surface coverage. For this, the rate of AFP adsorption on ice surface should be higher than the growth rate of the ice crystal plane. Very low concentration of AFP causes engulfment of ice bound proteins. Drori et al. reported similar adsorption rates for rQAE and TmAFP at the prism plane. , however adsorption to basal plane of TmAFP was much slower. The relatively slow hypAFP adsorption at the basal planes is observable at minor supercooling and thus modest ice growth rates[67].

The AFP samples demonstrated in the current study (AFPI-III, A20L and Tis8) form the following sequence when they are arranged in decreasing order of adsorption area on ice crystal surface: Tis8 > AFPII > AFPIII > AFPI > A20L. The obtained ranking is similar when we compared their IRI efficiency. So, it can be said that the binding ability of AFP to a wider area on ice crystal surface increases the IRI efficiency. It can also be predicted that IRI ability of one antifreeze protein can be improved by introducing a constructive mutation into the AFPs to expand their adsorption area on the ice crystal surface.

4.6 Correlation of IRI Activities of AFPs` with the Size of IBS:

Budke et al. (2014) reported that AFGP are by far the most effective IRI agents. The particular efficacy may be due to their disaccharide moieties. This supposition is supported by the fact that IRI efficacy is strongly reduced for monosaccharide AFGP analogues, as well as for AFGP analogues with acetyl-protected monosaccharide moieties. The author assumed that the molecular mass effect on efficacy is not merely due to the size of the molecule that causes a larger ice surface area covered per molecule, but also due to the larger molecules that represent more potential moieties for the adsorption to the ice which may cause faster or/and stronger adsorption to ice[13].

The approximate molecular weights of the AFP samples in the current study are as follows: 3.5 kDa (AFPI), 14 kDa (AFPII), 6.5 kDa (AFPIII), 6.5 kDa (A20L) and Tis8 (22 kDa).

The information of putative ice-binding residues and structural coordinates provided the relative size of ice binding site of each AFP: 1544 $Å^2$ (Tis8), 1149 $Å^2$ (AFPII), 820 $Å^2$ (AFPIII), 696 $Å^2$ (A20L) and 564 $Å^2$ (AFPI).

4.7 Effect of Salt on AFPs` IRI Activity:

Previous work suggested that the IRI efficiency is enhanced when the AFP is dissolved in several types of salts which causes the attaining of IRI endpoint at lower endpoint. Various AFPs have showed above phenomenon (Table 4.2). For example, Yu et al, (2010) reported that the IRI endpoint of ocean pout AFPIII is 98 nM and 780 nm in presence of 0.1 M ammonium bicarbonate buffer (pH 7.9) or Tris-buffered saline (150 mM NaCl and 10 mM Tris-HCl) (pH 7.5)[65]. The IRI endpoint of Sea raven AFPII in presence of Tris-buffered saline was found 0.16 μM[65].

On the other hand, Olijve et al found IRI endpoint 5.9 μM (5900 nM) for the same AFP in presence of 30% sucrose[67].

This kind of phenomenon might arise from the dissolved ions which are assumed to recruit water molecules around themselves and reduce the amount of freezable waters that can join the ice crystal. This may lead to reduction of AFP consumption to halt the ice growth[65].

4.8 Conclusion:

All the above insights provide a detail understanding of the underlying mechanism that governs IRI and TH activity, which supports the development of synthetic macromolecular antifreezes for cryoprotection, cryopreservation, deicing, and antiicing technologies[67].

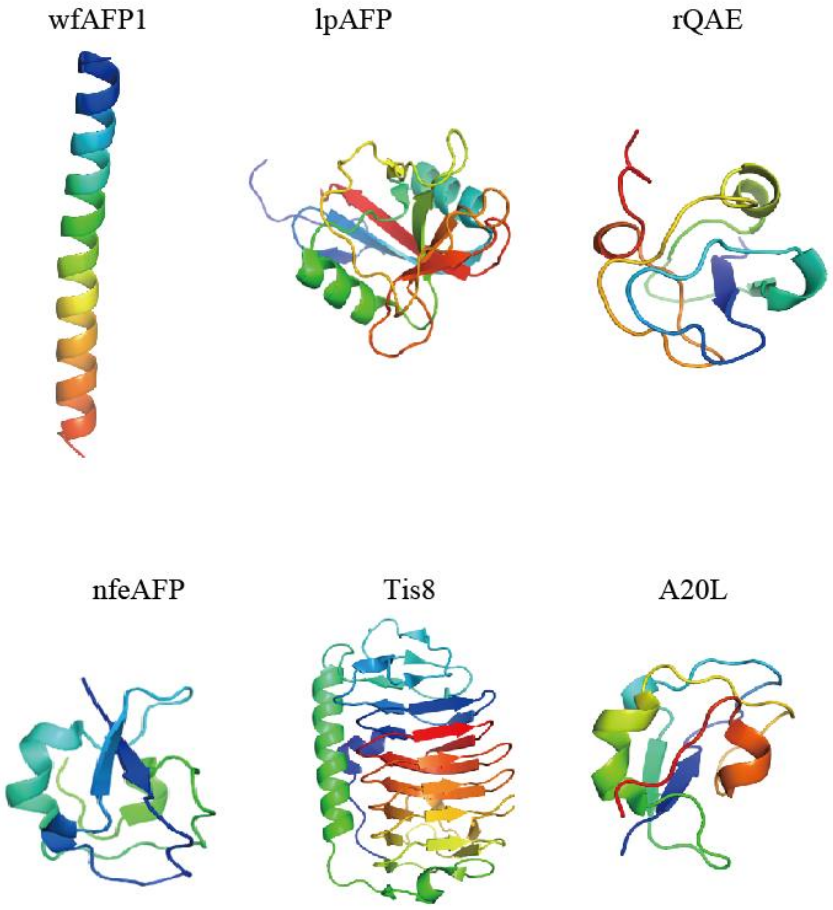

Figure 4.1: Different types of AFPs exhibiting IRI activity.

Table 4.1: Comparison of IRI activity between different AFPs.

AFP	Ice Crystal-Binding Plane	Ci, μM
AFPI	Pyramidal Planes (wfAFPI, recombinant) (67)	5.8 (67)
	Secondary Prism Planes, Pyramidal Planes (bpAFP, native) (Fig. 3.6)	4.69 (Fig. 3.6)
AFPII	Whole Planes Except Basal Planes(Fig. 3.6)	0.60 (Fig. 3.6)
AFPIII	Primary Prism Planes, Pyramidal Planes (67, Fig 3.6)	5.90 (rQAE, recombinant) (67)
		3.00 (nfeAFP, native) (Fig. 3.6)
Tis8	Whole Ice Plane (Fig. 3.6)	0.27 (Fig. 3.6)
A20L	Pyramidal Planes (Fig. 3.6)	7.69 (Fig. 3.6)

Table 4.2: Effect of solutes on IRI endpoints of various AFPs.

AFP	IRI Endpoint (nM)	
	0.1 M NH_4CO_3 (pH 7.9)	**TBS (pH 7.5)**
Winter flounder type I	195	1560
	195	1560
	195	3130
	391	3130
Sea raven type II	49	162
	49	391
	81	391
	98	391
Ocean pout type III	98	780
	98	780
	195	780
	391	780
MpAFP	-	391
		391
		391
		780
TmAFP	195	1600
	391	1850
	780	1850
	780	1950
	780	195
CfAFP	49	391
	49	780
	98	780
	98	780
		1190

References:

1. DL, N. *Lehninger`s Principles of Biochemistry*. (2005).
2. Pearson, B. C. *Biology*. (2008).
3. Rampelotto, P. Extremophiles and Extreme Environments. *Life* **3,** 482–485 (2013).
4. Feller, G. & Gerday, C. Psychrophilic enzymes: Hot topics in cold adaptation. *Nat. Rev. Microbiol.* **1,** 200–208 (2003).
5. Berthold, P. Migration: The biology of life on the move. *Endeavour* **21,** 42 (1997).
6. Doucet, D., Walker, V. K. & Qin, W. The bugs that came in from the cold: Molecular adaptations to low temperatures in insects. *Cellular and Molecular Life Sciences* **66,** 1404–1418 (2009).
7. Yeh, Y. & Feeney, R. E. Antifreeze Proteins: Structures and Mechanisms of Function. *Chem. Rev.* **96,** 601–618 (1996).
8. Oude Vrielink, A. S., Aloi, A., Olijve, L. L. C. & Voets, I. K. Interaction of ice binding proteins with ice, water and ions. *Biointerphases* **11,** 18906 (2016).
9. DeVries, A. L. & Wohlschlag, D. E. Freezing resistance in some antarctic fishes. *Science (80-.).* **163,** 1073–1075 (1969).
10. Knight, C. A., Cheng, C. C. & DeVries, A. L. Adsorption of alpha-helical antifreeze peptides on specific ice crystal surface planes. *Biophys. J.* **59,** 409–418 (1991).

11. Scotter, A. J. *et al.* The basis for hyperactivity of antifreeze proteins. *Cryobiology* **53,** 229–239 (2006).

12. Hassas-Roudsari, M. & Goff, H. D. Ice structuring proteins from plants: Mechanism of action and food application. *Food Research International* **46,** 425–436 (2012).

13. Budke, C. *et al.* Quantitative efficacy classification of ice recrystallization inhibition agents. *Cryst. Growth Des.* **14,** 4285–4294 (2014).

14. Capicciotti, C. J. *et al.* Small molecule ice recrystallization inhibitors enable freezing of human red blood cells with reduced glycerol concentrations. *Sci. Rep.* **5,** (2015).

15. Zachariassen, K. E. & Kristiansen, E. Ice nucleation and antinucleation in nature. *Cryobiology* **41,** 257–279 (2000).

16. Garnham, C. P. *et al.* A Ca^{2+} -dependent bacterial antifreeze protein domain has a novel β-helical ice-binding fold. *Biochem. J.* **411,** 171–180 (2008).

17. Gilbert, J. A., Davies, P. L. & Laybourn-Parry, J. A hyperactive, Ca 2+ -dependent antifreeze protein in an Antarctic bacterium. *FEMS Microbiol. Lett.* **245,** 67–72 (2005).

18. Guo, S., Garnham, C. P., Whitney, J. C., Graham, L. A. & Davies, P. L. Re-Evaluation of a Bacterial Antifreeze Protein as an Adhesin with Ice-Binding Activity. *PLoS One* **7,** (2012).

19. Vance, T. D. R. *et al.* Ca $^{2+}$ -stabilized adhesin helps an Antarctic bacterium reach out and bind ice. *Biosci. Rep.* **34,** 357–368 (2014).

20. Chen, L., DeVries, A. L. & Cheng, C.-H. C. Convergent evolution of antifreeze glycoproteins in Antarctic notothenioid fish and Arctic cod. *Proc. Natl. Acad. Sci.* **94,** 3817–3822 (1997).

21. Logsdon, J. M. & Doolittle, W. F. Origin of antifreeze protein genes - a cool tale in molecular evolution. *Proc. Natl. Acad. Sci. U. S. A.* **94,** 3485–3487 (1997).

22. Kim, H. J. *et al.* Marine antifreeze proteins: Structure, function, and application to cryopreservation as a potential cryoprotectant. *Mar. Drugs* **15,** (2017).

23. Fletcher, G. L., Hew, C. L. & Davies, P. L. Antifreeze proteins of teleost fishes. *Annu. Rev. Physiol.* **63,** 359–390 (2001).

24. Yang, D. S. C., Sax, M., Chakrabartty, A. & Hew, C. L. Crystal structure of an antifreeze polypeptide and its mechanistic implications. *Nature* **333,** 232–237 (1988).

25. Sicheri, F. & Yang, D. S. C. Ice-binding structure and mechanism of an antifreeze protein from winter flounder. *Nature* **375,** 427–431 (1995).

26. Marshall, C. B., Fletcher, G. L. & Davies, P. L. Hyperactive antifreeze protein in a fish. *Nature* **429,** 153 (2004).

27. Sun, T. *et al.* An antifreeze protein folds with an interior network of more than 400 semi-clathrate waters. *Science (80-.).* **343,** 795–798

(2014).

28. Sönnichsen, F. D., DeLuca, C. I., Davies, P. L. & Sykes, B. D. Refined solution structure of type III antifreeze protein: Hydrophobic groups may be involved in the energetics of the protein-ice interaction. *Structure* **4,** 1325–1337 (1996).

29. Jia, Z., DeLuca, C. I., Chao, H. & Davies, P. L. Structural basis for the binding of a globular antifreeze protein to ice. *Nature* **384,** 285–288 (1996).

30. Deng, G., Andrews, D. W. & Laursen, R. A. Amino acid sequence of a new type of antifreeze protein, from the longhorn sculpin Myoxocephalus octodecimspinosis. *FEBS Lett.* **402,** 17–20 (1997).

31. Gauthier, S. Y. *et al.* A re-evaluation of the role of type IV antifreeze protein. *Cryobiology* **57,** 292–296 (2008).

32. Liou, Y. C., Tocilj, A., Davies, P. L. & Jia, Z. Mimicry of ice structure by surface hydroxyls and water of a ??-helix antifreeze protein. *Nature* **406,** 322–324 (2000).

33. Gauthier, S. Y., Kay, C. M., Sykes, B. D., Walker, V. K. & Davies, P. L. Disulfide bond mapping and structural characterization of spruce budworm antifreeze protein. *Eur. J. Biochem.* **258,** 445–453 (1998).

34. Graethert, S. P. *et al.* β-Helix structure and ice-binding properties of a hyperactive antifreeze protein from an insect. *Nature* **406,** 325–328 (2000).

35. Li, C., Guo, X., Jia, Z., Xia, B. & Jin, C. Solution structure of an antifreeze protein CfAFP-501 from choristoneura fumiferana. *J. Biomol. NMR* **32,** 251–256 (2005).

36. Lin, F. H., Davies, P. L. & Graham, L. A. The Thr- and ala-rich hyperactive antifreeze protein from inchworm folds as a flat silk-like ??-Helix. *Biochemistry* **50,** 4467–4478 (2011).

37. Graham, L. A. & Davies, P. L. Biochemistry: Glycine-rich antifreeze proteins from snow fleas. *Science (80-.).* **310,** 461 (2005).

38. Pentelute, B. L. *et al.* X-ray structure of snow flea antifreeze protein determined by racemic crystallization of synthetic protein enantiomers. *J. Am. Chem. Soc.* **130,** 9695–9701 (2008).

39. Mok, Y. F. *et al.* Structural Basis for the Superior Activity of the Large Isoform of Snow Flea Antifreeze Protein. *Biochemistry* **49,** 2593–2603 (2010).

40. Kristiansen, E., Pedersen, S., Zachariassen, K. E. & Ramløv, H. Antifreeze activity in the cerambycid beetle Rhagium inquisitor. *J. Comp. Physiol. - B Biochem. Syst. Environ. Physiol.* **169,** 55–60 (1999).

41. Kristiansen, E. *et al.* Structural characteristics of a novel antifreeze protein from the longhorn beetle Rhagium inquisitor. *Insect Biochem. Mol. Biol.* **41,** 109–117 (2011).

42. Basu, K., Graham, L. A., Campbell, R. L. & Davies, P. L. Flies expand the repertoire of protein structures that bind ice. *Proc. Natl. Acad. Sci.* **112,** 737–742 (2015).

43. Raymond, J. A., Fritsen, C. & Shen, K. An ice-binding protein from an Antarctic sea ice bacterium. *FEMS Microbiol. Ecol.* **61,** 214–221 (2007).

44. Sun, X., Griffith, M., Pasternak, J. J. & Glick, B. R. Low temperature growth, freezing survival, and production of antifreeze protein by the plant growth promoting rhizobacterium Pseudomonas putida GR12-2. *Can. J. Microbiol.* **41,** 776–784 (1995).

45. Xu, H., Griffith, M., Patten, C. L. & Glick, B. R. Isolation and characterization of an antifreeze protein with ice nucleation activity from the plant growth promoting rhizobacterium Pseudomonas putida GR12-2. *Can. J. Microbiol.* **44,** 64–73 (1998).

46. Yamashita, Y. *et al.* Identification of an antifreeze lipoprotein from Moraxella sp. of Antarctic origin. *Biosci. Biotechnol. Biochem.* **66,** 239–247 (2002).

47. Kawahara, H. *et al.* Production of two types of ice crystal-controlling proteins in antarctic bacterium. *J. Biosci. Bioeng.* **98,** 220–223 (2004).

48. Garnham, C. P., Campbell, R. L. & Davies, P. L. Anchored clathrate waters bind antifreeze proteins to ice. *Proc. Natl. Acad. Sci.* **108,** 7363–7367 (2011).

49. Do, H., Lee, J. H., Lee, S. G. & Kim, H. J. Crystallization and preliminary X-ray crystallographic analysis of an ice-binding protein (FfIBP) from Flavobacterium frigoris PS1. *Acta Crystallogr. Sect. F Struct. Biol. Cryst. Commun.* **68,** 806–809 (2012).

50. Jia, Z. & Davies, P. L. Antifreeze proteins: An unusual receptor-ligand

interaction. *Trends in Biochemical Sciences* **27,** 101–106 (2002).

51. Do, H. *et al.* Structure-based characterization and antifreeze properties of a hyperactive ice-binding protein from the Antarctic bacterium Flavobacterium frigoris PS1. *Acta Crystallogr. Sect. D Biol. Crystallogr.* **70,** 1061–1073 (2014).

52. Hanada, Y., Nishimiya, Y., Miura, A., Tsuda, S. & Kondo, H. Hyperactive antifreeze protein from an Antarctic sea ice bacterium Colwellia sp. has a compound ice-binding site without repetitive sequences. *FEBS J.* **281,** 3576–3590 (2014).

53. Raymond, J. A. & Kim, H. J. Possible role of horizontal gene transfer in the colonization of sea ice by Algae. *PLoS One* **7,** (2012).

54. Pucciarelli, S. *et al.* Identification and analysis of two sequences encoding ice-binding proteins obtained from a putative bacterial symbiont of the psychrophilic Antarctic ciliate Euplotes focardii. *Antarct. Sci.* **26,** 491–501 (2014).

55. Mangiagalli, M. *et al.* Cryo-protective effect of an ice-binding protein derived from Antarctic bacteria. *FEBS J.* **284,** 163–177 (2017).

56. Singh, P., Hanada, Y., Singh, S. M. & Tsuda, S. Antifreeze protein activity in Arctic cryoconite bacteria. *FEMS Microbiology Letters* **351,** 14–22 (2014).

57. Lee, J. K. *et al.* An extracellular ice-binding glycoprotein from an Arctic psychrophilic yeast. *Cryobiology* **60,** 222–228 (2010).

58. Raymond, J. A., Christner, B. C. & Schuster, S. C. A bacterial ice-binding protein from the Vostok ice core. *Extremophiles* **12,** 713–717 (2008).

59. Xiao, N. *et al.* Comparison of functional properties of two fungal antifreeze proteins from Antarctomyces psychrotrophicus and Typhula ishikariensis. *FEBS J.* **277,** 394–403 (2010).

60. Shah, S. H. H. *et al.* Solution Structures, Dynamics, and Ice Growth Inhibitory Activity of Peptide Fragments Derived from an Antarctic Yeast Protein. *PLoS One* **7,** (2012).

61. Sidebottom, C. *et al.* Heat-stable antifreeze protein from grass. *Nature* **406,** 256 (2000).

62. Worrall, D. *et al.* A carrot leucine-rich-repeat protein that inhibits ice recrystallization. *Science (80-.).* **282,** 115–117 (1998).

63. Zhang, D. Q., Liu, B., Feng, D. R., He, Y. M. & Wang, J. F. Expression, purification, and antifreeze activity of carrot antifreeze protein and its mutants. *Protein Expr. Purif.* **35,** 257–263 (2004).

64. Middleton, A. J. *et al.* Antifreeze protein from freeze-tolerant grass has a beta-roll fold with an irregularly structured ice-binding site. *J. Mol. Biol.* **416,** 713–724 (2012).

65. Yu, S. O. *et al.* Ice restructuring inhibition activities in antifreeze proteins with distinct differences in thermal hysteresis. *Cryobiology* **61,** 327–334 (2010).

66. Graham, L. A., Liou, Y. C., Walker, V. K. & Davies, P. L. Hyperactive antifreeze protein from beetles [8]. *Nature* **388,** 727–728 (1997).

67. Olijve, L. L. C. *et al.* Blocking rapid ice crystal growth through nonbasal plane adsorption of antifreeze proteins. *Proc. Natl. Acad. Sci.* **113,** 3740–3745 (2016).

68. Raymond, J. a, Wilson, P. & DeVries, a L. Inhibition of growth of nonbasal planes in ice by fish antifreezes. *Proc. Natl. Acad. Sci. U. S. A.* **86,** 881–885 (1989).

69. Mahatabuddin, S. *et al.* Concentration-dependent oligomerization of an alpha-helical antifreeze polypeptide makes it hyperactive. *Sci. Rep.* **7,** 42501 (2017).

70. Kay, C. M., Sykes, B. D., Loewen, M. C. & Davies, P. L. A diminished role for hydrogen bonds in antifreeze protein binding to ice. *Biochemistry* (1997).

71. Haymet, A. D. J., Ward, L. G., Harding, M. M. & Knight, C. A. Valine substituted winter flounder 'antifreeze': Preservation of ice growth hysteresis. *FEBS Lett.* **430,** 301–306 (1998).

72. Sonnichsen, F. D., Sykes, B. D. & Davies, P. L. Comparative modeling of the three-dimensional structure of type II antifreeze protein. *Protein Sci* **4,** 460–471 (1995).

73. Nutt, D. R. & Smith, J. C. Dual function of the hydration layer around an antifreeze protein revealed by atomistic molecular dynamics simulations. *J. Am. Chem. Soc.* **130,** 13066–13073 (2008).

74. Garnham, C. P., Nishimiya, Y., Tsuda, S. & Davies, P. L. Engineering a naturally inactive isoform of type III antifreeze protein into one that can stop the growth of ice. *FEBS Lett.* **586,** 3876–3881 (2012).

75. Sun, T., Gauthier, S. Y., Campbell, R. L. & Davies, P. L. Revealing Surface Waters on an Antifreeze Protein by Fusion Protein Crystallography Combined with Molecular Dynamic Simulations. *J. Phys. Chem. B* **119,** 12808–12815 (2015).

76. Garnham, C. P. *et al.* Compound ice-binding site of an antifreeze protein revealed by mutagenesis and fluorescent tagging. *Biochemistry* **49,** 9063–9071 (2010).

77. Basu, K. *et al.* Determining the ice-binding planes of antifreeze proteins by fluorescence-based ice plane affinity. *J. Vis. Exp.* e51185 (2014). doi:10.3791/51185

78. Nishimiya, Y. *et al.* Crystal Structure and Mutational Analysis of Ca2+-Independent Type II Antifreeze Protein from Longsnout Poacher, Brachyopsis rostratus. *J. Mol. Biol.* **382,** 734–746 (2008).

79. Davies, P. L. & Hew, C. L. Biochemistry of fish antifreeze proteins. *FASEB J.* **4,** 2460–2468 (1990).

80. HEW, C. L. & YANG, D. S. C. Protein interaction with ice. *Eur. J. Biochem.* **203,** 33–42 (1992).

81. Davies, P. L., Baardsnes, J., Kuiper, M. J. & Walker, V. K. Structure and function of antifreeze proteins. *Philos. Trans. R. Soc. Lond. B. Biol. Sci.* **357,** 927–935 (2002).

82. Takamichi, M., Nishimiya, Y., Miura, A. & Tsuda, S. Effect of annealing time of an ice crystal on the activity of type III antifreeze protein. *FEBS J.* **274,** 6469–76 (2007).

83. Martino, M. N. & Zaritzky, N. E. Ice recrystallization in a model system and in frozen muscle tissue. *Cryobiology* **26,** 138–148 (1989).

84. Wu, S. *et al.* Ion-specific ice recrystallization provides a facile approach for the fabrication of porous materials. *Nat. Commun.* **8,** (2017).

85. Knight, C. A., Hallett, J. & DeVries, A. L. Solute effects on ice recrystallization: An assessment technique. *Cryobiology* **25,** 55–60 (1988).

86. Tomczak, M. M., Marshall, C. B., Gilbert, J. A. & Davies, P. L. A facile method for determining ice recrystallization inhibition by antifreeze proteins. *Biochem. Biophys. Res. Commun.* **311,** 1041–1046 (2003).

87. Lotze, S. *et al.* Communication: Probing the absolute configuration of chiral molecules at aqueous interfaces. *J. Chem. Phys.* **143,** (2015).

88. Jackman, J. *et al.* Assessing antifreeze activity of AFGP 8 using domain recognition software. *Biochem. Biophys. Res. Commun.* **354,** 340–344 (2007).

89. Olijve, L. L. C., Oude Vrielink, A. S. & Voets, I. K. A simple and quantitative method to evaluate ice recrystallization kinetics using the circle hough transform algorithm. *Cryst. Growth Des.* **16,** 4190–4195 (2016).

90. Graham, L. A., Agrawal, P., Oleschuk, R. D. & Davies, P. L. High-capacity ice-recrystallization endpoint assay employing superhydrophobic coatings that is equivalent to the 'splat' assay. *Cryobiology* **81,** 138–144 (2018).

91. Dalal, P. & Sönnichsen, F. D. Source of the ice-binding specificity of antifreeze protein type I. *J. Chem. Inf. Comput. Sci.* **40,** 1276–1284 (2000).

92. Davies, P. L. Ice-binding proteins: A remarkable diversity of structures for stopping and starting ice growth. *Trends in Biochemical Sciences* **39,** 548–555 (2014).

93. Hobbs, P. V. Ice Physics. in *Ice Physics* 461–571 (1974). doi:10.1002/ejoc.201200111

94. Liu, Y. *et al.* Structure and Evolutionary Origin of Ca 2+ -Dependent Herring Type II Antifreeze Protein. *Structure* **2,** e548 (2007).

95. Deng, G. & Laursen, R. A. Isolation and characterization of an antifreeze protein from the longhorn sculpin, Myoxocephalus octodecimspinosis. *Biochim. Biophys. Acta* **1388,** 305–314 (1998).

96. Knight, C. A. & DeVries, A. L. Effects of a polymeric, nonequilibrium 'antifreeze' upon ice growth from water. *J. Cryst. Growth* **143,** 301–310 (1994).

97. Park, K. S. *et al.* Characterization of the ice-binding protein from Arctic yeast Leucosporidium sp. AY30. *Cryobiology* **64,** 286–296 (2012).

98. Pertaya, N., Marshall, C. B., Celik, Y., Davies, P. L. & Braslavsky, I. Direct visualization of spruce budworm antifreeze protein interacting with ice crystals: Basal plane affinity confers hyperactivity. *Biophys. J.* **95,** 333–341 (2008).

99. Hakim, A. *et al.* Crystal structure of an insect antifreeze protein and its implications for ice binding. *J. Biol. Chem.* **288,** 12295–12304 (2013).

100. Kondo, H. *et al.* Ice-binding site of snow mold fungus antifreeze protein deviates from structural regularity and high conservation. *Proc. Natl. Acad. Sci.* **109,** 9360–9365 (2012).

101. Middleton, A. J., Brown, A. M., Davies, P. L. & Walker, V. K. Identification of the ice-binding face of a plant antifreeze protein. *FEBS Lett.* **583,** 815–819 (2009).

102. Marshall, C. B., Daley, M. E., Sykes, B. D. & Davies, P. L. Enhancing the activity of a β-helical antifreeze protein by the engineered addition of coils. *Biochemistry* **43,** 11637–11646 (2004).

103. Leinala, E. K. *et al.* A β-helical antifreeze protein isoform with increased activity. Structural and functional insights. *J. Biol. Chem.* **277,** 33349–33352 (2002).

104. Balcerzak, A. K., Capicciotti, C. J., Briard, J. G. & Ben, R. N. Designing ice recrystallization inhibitors: from antifreeze (glyco)proteins to small molecules. *RSC Adv.* **4,** 42682–42696 (2014).

105. Capicciotti, C. J., Malay, D. & Ben, R. N. Ice Recrystallization Inhibitors: From Biological Antifreeze to Small Molecules. in *Recent*

Developments in the Study of Recrystallization 177–224 (2013). doi:http://dx.doi.org/10.5772/54992

106. Hartel, R. W. The properties of water in foods. *(Blackie Acad. Profssional, London)* (1998).

107. Hartel, R. W. Crystallization in foods. *(Aspen Publ. Gaithersburg)* (2001).

108. Hagiwara, T., Hartel, R. W. & Matsukawa, S. Relationship between recrystallization rate of ice crystals in sugar solutions and water mobility in freeze-concentrated matrix. *Food Biophys.* **1,** 74–82 (2006).

109. Graham, B., Fayter, A. E. R., Houston, J. E., Evans, R. C. & Gibson, M. I. Facially Amphipathic Glycopolymers Inhibit Ice Recrystallization. *J. Am. Chem. Soc.* **140,** 5682–5685 (2018).

110. Voets, I. K. From ice-binding proteins to bio-inspired antifreeze materials. *Soft Matter* **13,** 4808–4823 (2017).

111. Nishimiya, Y., Sato, R., Takamichi, M., Miura, A. & Tsuda, S. Co-operative effect of the isoforms of type III antifreeze protein expressed in Notched-fin eelpout, Zoarces elongatus Kner. *FEBS J.* **272,** 482–492 (2005).

112. Smallwood, M. *et al.* Isolation and characterization of a novel antifreeze protein from carrot (Daucus carota). *Biochem. J.* **340,** 385–391 (1999).

113. Budke, C., Heggemann, C., Koch, M., Sewald, N. & Koop, T. Ice recrystallization kinetics in the presence of synthetic antifreeze

glycoprotein analogues using the framework of LSW theory. *J. Phys. Chem. B* **113,** 2865–2873 (2009).

114. Dreischmeier, K., Budke, C., Wiehemeier, L., Kottke, T. & Koop, T. Boreal pollen contain ice-nucleating as well as ice-binding 'antifreeze' polysaccharides. *Sci. Rep.* **7,** (2017).

115. Briard, J. G. *et al.* Small molecule ice recrystallization inhibitors mitigate red blood cell lysis during freezing, transient warming and thawing. *Sci. Rep.* **6,** (2016).

116. Mitchell, D. E. & Gibson, M. I. Latent Ice Recrystallization Inhibition Activity in Nonantifreeze Proteins: Ca2+-Activated Plant Lectins and Cation-Activated Antimicrobial Peptides. *Biomacromolecules* **16,** 3411–3416 (2015).

117. Duman, J. G., Bennett, V., Sformo, T., Hochstrasser, R. & Barnes, B. M. Antifreeze proteins in Alaskan insects and spiders. *J. Insect Physiol.* **50,** 259–266 (2004).

118. Duman, J. G. & Olsen, T. M. Thermal hysteresis protein activity in bacteria, fungi, and phylogenetically diverse plants. *Cryobiology* **30,** 322–328 (1993).

119. Raymond, J. A. & DeVries, A. L. Adsorption inhibition as a mechanism of freezing resistance in polar fishes. *Proc. Natl. Acad. Sci. U. S. A.* **74,** 2589–2593 (1977).

120. Celik, Y. *et al.* Superheating of ice crystals in antifreeze protein solutions. *Proc. Natl. Acad. Sci. U. S. A.* **107,** 5423–8 (2010).

121. Kristiansen, E. & Zachariassen, K. E. The mechanism by which fish antifreeze proteins cause thermal hysteresis. *Cryobiology* **51,** 262–280 (2005).

122. Basu, K. *et al.* Determining the Ice-binding Planes of Antifreeze Proteins by Fluorescence-based Ice Plane Affinity. *J. Vis. Exp.* (2014). doi:10.3791/51185

123. Mahatabuddin, S. *et al.* Polypentagonal ice-like water networks emerge solely in an activity-improved variant of ice-binding protein. *Proc. Natl. Acad. Sci.* **115,** 5456–5461 (2018).

124. Cheng, J., Hanada, Y., Miura, A., Tsuda, S. & Kondo, H. Hydrophobic ice-binding sites confer hyperactivity of an antifreeze protein from a snow mold fungus. *Biochem. J.* **473,** 4011–4026 (2016).

125. Baardsnes, J. *et al.* New ice-binding face for type I antifreeze protein. *FEBS Lett.* **463,** 87–91 (1999).

126. Winn, M. D. *et al.* Overview of the CCP4 suite and current developments. *Acta Crystallographica Section D: Biological Crystallography* **67,** 235–242 (2011).

127. Beirão, J. *et al.* Improving sperm cryopreservation with antifreeze proteins: effect on gilthead seabream (Sparus aurata) plasma membrane lipids. *Biol. Reprod.* **86,** 59 (2012).

128. Nishijima, K. *et al.* Effects of type III antifreeze protein on sperm and embryo cryopreservation in rabbit. *Cryobiology* **69,** 22–25 (2014).

129. Qadeer, S. *et al.* Evaluation of antifreeze protein III for cryopreservation of Nili-Ravi (Bubalus bubalis) buffalo bull sperm. *Anim. Reprod. Sci.* **148,** 26–31 (2014).

130. DeLano, W. L. PyMOL: An open-source molecular graphics tool. *CCP4 Newsl. Protein Crystallogr.* **40,** 82–92 (2002).

Accomplishments

Original manuscripts:

(i) Rahman AT, Arai T, Yamauchi A, Miura A, Kondo H, Ohyama Y and Tsuda S "Ice recrystallization is strongly inhibited when antifreeze proteins bind to multiple ice planes." Accepted in Nature scientific Reports, waiting for online publication.

(ii) Rahman AT, Miura A, Kondo H and Tsuda S "A critical review of the mechanics of ice recrystallization." (Manuscript in preparation)

(v) Khan NMMU, Rahman AT, Arai T, Watanabe A, Tsuda S, Kondo H: "Site-directed Mutagenesis Improves the Activity of a Moderately Active Fungal Antifreeze Protein" (Manuscript in preparation)

Conference Presentations:

(i) Rahman AT, Mahatabuddin S, Ohyama Y, Kondo H and Tsuda S: "Quantitative methods to evaluate ice recrystallization inhibition rate using Ferret's diameter" *The 4th International Life Science Symposium*, Conference hall of Hokkaido University, Sapporo, Japan; 18 November/2016. (Poster presentation)

(ii) Rahman AT, Mahatabuddin S, Ohyama Y, Kondo H and Tsuda S: "Quantitative Method to Evaluate Ice Recrystallization Kinetics of AFP Solutions" 26th Chemical Engineering Conference, Hokkaido University, Sapporo, Japan; 27 January/2017. (Oral presentation)

(iii) Rahman AT, Mahatabuddin S, Ohyama Y, Kondo H and Tsuda S: "Quantitative Methods to Evaluate Ice Recrystallization Kinetics of AFP Solutions" *The 5th International Life Science Symposium*, Conference hall of Hokkaido University, Sapporo, Japan; 28 October/2017. (Oral presentation)

(iv) Rahman AT, Arai T, Yamauchi A, Miura A, Kondo H, Ohyama Y, Tsuda S: "Strength of ice recrystallization is maximized by whole ice-coverage of antifreeze protein" *The 6th International Life Science Symposium*, Conference hall of Hokkaido University, Sapporo, Japan; 19 November/2018. (Poster presentation)

(v) Khan NMMU, Rahman AT, Arai T, Watanabe A, Tsuda S, Kondo H: "Site-directed Mutagenesis Improves the Activity of a Moderately Active Fungal Antifreeze Protein" *The 6th International Life Science Symposium*, Conference hall of Hokkaido University, Sapporo, Japan; 19 November/2018. (Poster presentation)

Acknowledgements

At first, I would like to thank Prof. Sakae Tsuda, for accepting me as a PhD student. His valuable suggestions, support and guidance helped me carry out the work properly. It was a great opportunity for me to meet a scientist like him and working under his supervision was really enjoyable and memorable. It was his hopes that pinned on the lines of my skill and that's what led me forward. I owe to his my confidence in my ability to come forward thus far. I am grateful to Dr. Hidemasa Kondo for his kind, patient and instantaneous advices along with the technical guidance to perform experiments. I am thankful for his great supports to lead a daily life in Sapporo.

I am thankful for the instrumental setting and protein preparation to Dr. Sheikh Mahatabuddin and Tatsuya Arai. I am also thankful to Ms. Ai Miura for her fundamental and administrative supports. I am also very glad to all students in this lab for their accompanying, supporting and encouraging every day.

I am sincerely thankful to the **IGP-RPLS (International Graduate Program for Research Pioneers in Life Sciences)** and **Monbukagakusho: MEXT** for providing me all kinds of financial support.

I would like to express my sincere gratitude to my honorable formal teacher and supervisor Prof. Dr. Yearul Kabir, Department of Biochemistry & Molecular Biology, University of Dhaka, for his encouraging words and supports to make me interested on research. . I was lucky to get him as my supervisor and I feel honored to be his student.

I wish to express my gratitude to my family for their unlimited support during my thesis work. Additionally, I would also like to thank my Sapporo friends (Ena, Shazia, Papry, Jeny and Rumana) who gave me time in listening to me and helping me out my problems during my daily life in Japan.

Finally, I am grateful to almighty Allah who gave me the courage and patience for accomplishing the work for my thesis, with blessings, guidance, protection, help and wisdom in all spheres of my life.